TECHNICAL MEMORANDUM

133

ECMWF monitoring tools and their application to North American radiosonde data

H. Böttger, A. Radford
and D. Söderman

Operations Department

June 1987

European Centre for Medium-Range Weather Forecasts
Europäisches Zentrum für mittelfristige Wettervorhersage
Centre européen pour les prévisions météorologiques à moyen

1. INTRODUCTION

Much progress has been made in recent years in numerical weather forecasting. Models and analysis techniques have been developed and refined while the rapidly increasing power of supercomputers has actually enabled the scientists to implement their schemes. However, numerical forecasting is not only a modelling but also an initial data problem. At a recent meeting on data for global models (ECMWF, 1987) the need for an improved data coverage and better quality data was stressed. Much can be gained from improvements in the Global Observing System (GOS). However, very little has happened over the last few years. Instead of an improvement there are signs of a degradation of the system, in particular in the conventional surface based observations.

In order to manifest the deficiencies in the availability and quality of the observations, ECMWF undertakes regular data monitoring and has on various occasions made the results available to the WMO, data producers and other GDPS centres. WMO/CBS has endorsed such monitoring activities and recommended the exchange of results between monitoring centres (WMO, CBS EX(85)).

One of the most important conventional surface based data sets is provided by the global radiosonde network. Its performance has been studied in detail at ECMWF. Tools were developed to assess the long-term trend of data availability and quality at individual stations and to display the results in geographical maps to facilitate the comparison between stations. The purpose of this paper is to demonstrate the ECMWF monitoring tools and present examples of their application to the radiosonde network over North America. As the ECMWF data assimilation system provides the diagnostic facilities for the data monitoring, first a brief summary of the ECMWF operational system is given.

2. ECMWF OPERATIONAL ANALYSIS AND FORECAST SYSTEM

2.1 Schedule

ECMWF produces routine global analyses for the four main synoptic hours 00, 06, 12 and 18 UTC and global 10-day forecasts based on 12 UTC data. The operational schedule with the approximate running times of the analysis and forecast suite is shown in Fig. 1. As a forecasting centre with the emphasis on the medium-range, ECMWF operates with long data collection times of between 18

hours for the 18 UTC analysis and 8 hours for the 12 UTC final analysis. This schedule ensures the most comprehensive global data coverage including the Southern Hemisphere surface data and global satellite sounding data, thus obtaining the best possible description of the initial state of the atmosphere.

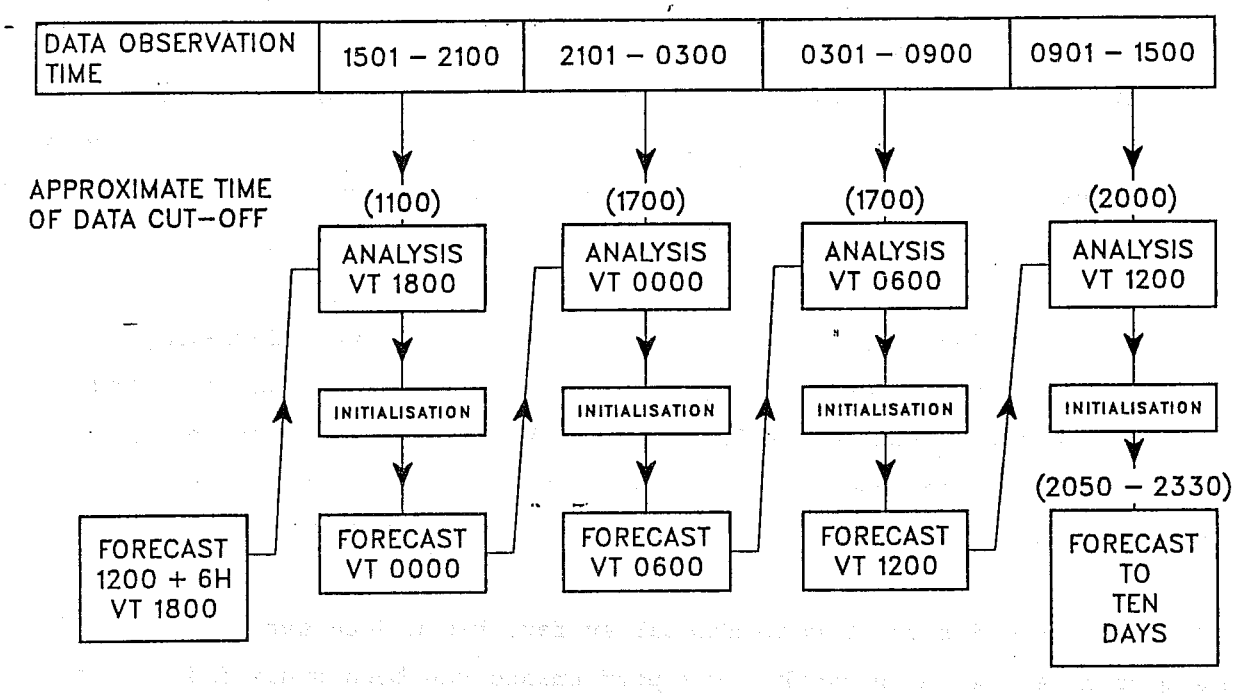

Fig. 1 ECMWF Operational Schedule

2.2 Data assimilation system

ECMWF operates a full data assimilation system with intermittent data insertion and three main steps: analysis, initialisation and 6-hour forecast to provide the first-guess for the next analysis. The system is described by Lorenc (1981) and the recent revisions of the analysis were documented by Shaw, Lönnberg and Hollingsworth (1984), and Lönnberg, Pailleux and Hollingsworth (1986). The present system is summarised in Fig. 2. A comprehensive quality control scheme for the data is included in the analysis (Lönnberg and Shaw, 1985). Prior to the use of the data in the analysis the incoming bulletins undergo telecommunications checks, decoding and simple checks on departure from rather wide climatological limits. The internal consistency of radiosonde data is controlled by applying the hydrostatic check.

2.3 The forecast model

The first-guess field is produced with the same operational forecast model that provides the main 10-day forecast. The resolution of the model is given by spectral representation which at present is truncated at wavenumber 106. Therefore features with a half wavelength of approximately 190 km can at best be expected to be resolved. Physical processes are calculated on the surface grid of the model which has a near regular resolution of 1.125 degrees in latitude and longitude. The main features of the model are presented in Fig. 3. For a more comprehensive description of the model and the physical parameterisation reference is made to Tiedtke et.al. (1979), Simmons and Jarraud (1983), Jarraud et.al. (1985), Tiedtke and Slingo (1985).

$P_{k+½}=A_{k+½}+B_{k+½}Ps$,

$A_{k+½}$(hPa)	$B_{k+½}$
10	0
20	0
40	0
60	0
83	0.004
106	0.014
128	0.035
146	0.072
158	0.127
161	0.202
153	0.296
136	0.405
111	0.524
82	0.645
52	0.759
26	0.856
8	0.929
0	0.973
0	0.992
0	1

Vertical Coordinate Table (NL=19)

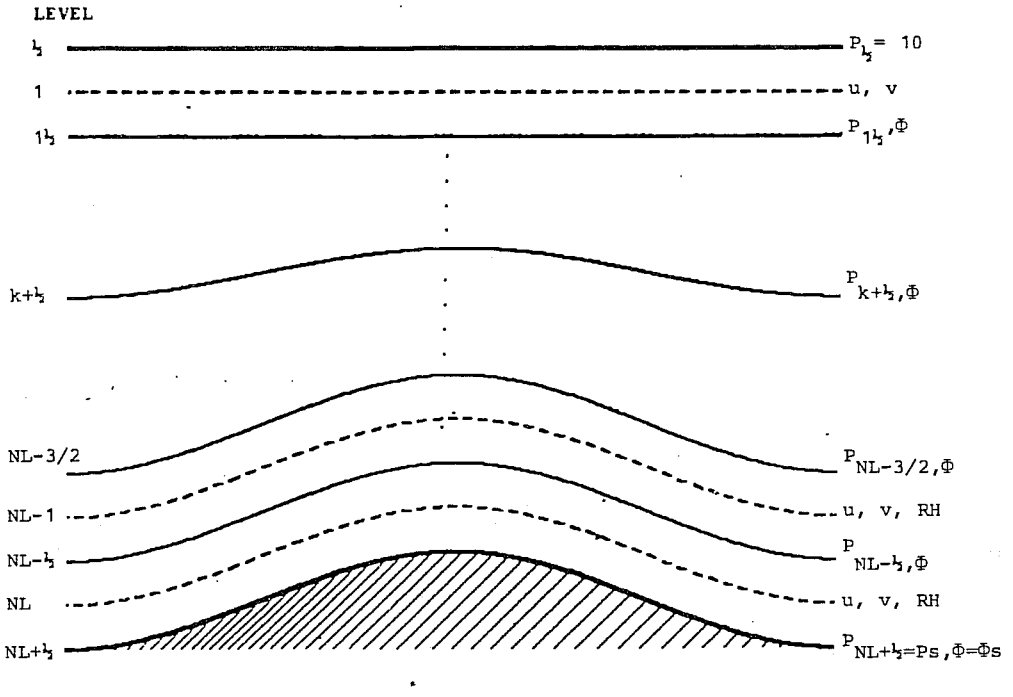

Disposition of variables in the vertical

Domain	Global
Data assimilation frequency	6-hr (± 3-hr observation time window)
First guess	6-hr forecast
Dependent variables	Ps, Φ, u, v, RH
Vertical coordinate	Hybrid, $P_{k+½}=A_{k+½}+B_{K+½}Ps$, details as above
Horizontal grid	160 x 320 points on a quasi-regular (1.125°) "Gaussian" grid
Analysis method	Mass and wind: 3-dimensional multi-variate statistical interpolation
	Relative humidity: 3-dimensional uni-variate statistical interpolation up to 250 hPa
	Surface: Sea surface temperature from NMC analysis
	Soil water content using rainfall observations, estimated evaporation
	Snow depth using snow depth and snowfall observations
Initialisation method	Non-linear normal mode, 5 vertical modes, non-adiabatic

Fig. 2 ECMWF Analysis System

$P_{k+\frac{1}{2}} = A_{k+\frac{1}{2}} + B_{k+\frac{1}{2}} P_s$,

$A_{k+\frac{1}{2}}$ (hPa)	$B_{k+\frac{1}{2}}$
0	0
20	0
40	0
60	0
83	0.004
106	0.014
128	0.035
146	0.072
158	0.127
161	0.202
153	0.296
136	0.405
111	0.524
82	0.645
52	0.759
26	0.856
8	0.929
0	0.973
0	0.992
0	1

Vertical Coordinate Table (NL=19)

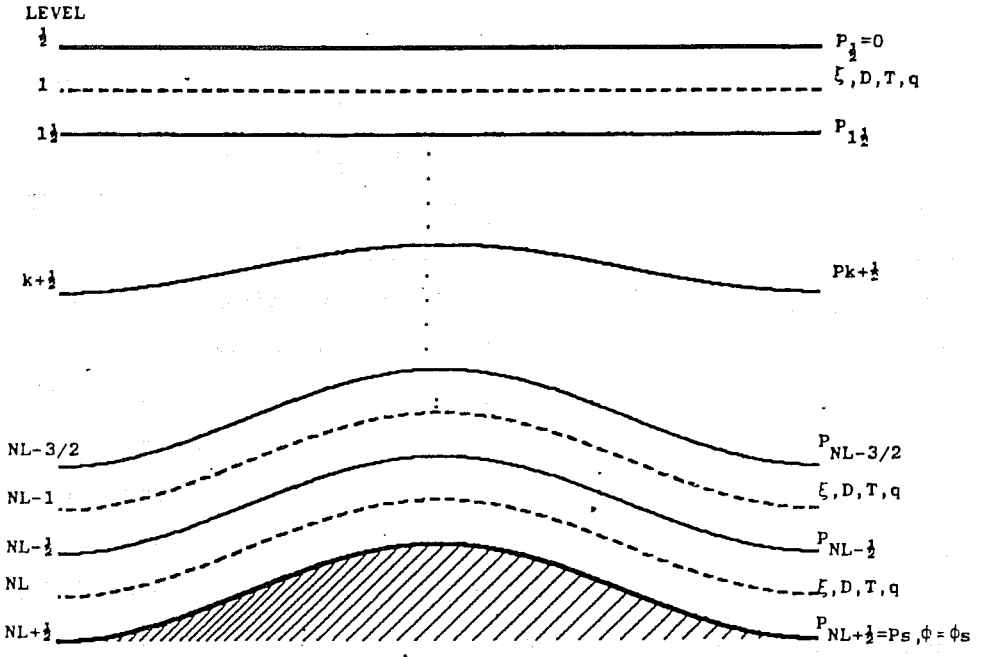

Disposition of variables in the vertical

Domain	Global
Initial data time	12Z
Dependent variables	$\xi, D, T, q, \ln(P_s)$
Vertical coordinate	Hybrid, $P_{k+\frac{1}{2}} = A_{k+\frac{1}{2}} + B_{k+\frac{1}{2}} P_s$, details as above.
Vertical representation	Finite-difference, energy and angular-momentum conserving.
Horizontal representation	Spectral, with triangular truncation at wavenumber 106.
Horizontal grid	160 x 320 points on a quasi-regular (1.125°) 'Gaussian' grid.
Time integration	Leapfrog, semi-implicit (Δt=15 min), time filter (ε=0.1)
Horizontal diffusion	Linear, fourth-order ($K=1 \times 10^{15} m^4 s^{-1}$)
Orography	Grid-scale average from high resolution data set, enhanced by one standard deviation of sub-grid scale orography, spectrally-fitted.
Vertical boundary conditions	Kinematic.
Physical parameterisation	(i) Boundary eddy fluxes dependent on local roughness length and stability (Monin-Obukov).
	(ii) Free-atmosphere turbulent fluxes dependent on mixing length and Richardson number.
	(iii) Kuo convection scheme. Shallow convection parameterised by an eddy mixing scheme.
	(iv) Interaction between radiation and model-generated clouds. Albedo dependent on model snow cover.
	(v) Large-scale condensation when grid-square saturated. Evaporation of precipitation.
	(vi) Computed land temperature with diurnal cycle (3 layers in soil).
	(vii) Computed soil moisture and snow cover.
	(viii) Fixed, analysed sea-surface temperature.
Statistical correction of forecasts	None

Fig. 3 ECMWF Forecast Model

3. OBSERVATION QUALITY MONITORING BY DATA ASSIMILATION

Hollingsworth et.al. (1986) provided the rationale for using modern data assimilation systems as the appropriate tools for monitoring the quality of observations. There is good evidence that in mid-latitude areas, where an adequate observational network ensures a sufficient data coverage, the 6-hour forecast error (first-guess error) is quite low and allows the evaluation of the data quality by comparison with the first-guess. North America, Europe and most parts of Asia are suitable areas for such evaluations. In data sparse areas, however, a more cautious approach is required, before any conclusions on the data quality are drawn from the comparison with the first-guess alone, as the model errors might be dominating. Only if additional independent comparisons, such as results from collocation statistics of radiosonde ascents and atmospheric soundings derived from satellite radiance measurements corroborate the data versus first-guess findings may they be accepted with confidence. ECMWF has developed such additional tools and applies them whenever possible to confirm monitoring results for radiosondes in data sparse areas, e.g. the Southern Hemisphere and mid-Pacific Islands.

4. RESULTS

In this section are presented the ECMWF monitoring results for the North American radiosonde network. Area statistics are displayed of

a) data availability (i.e. reception rate at ECMWF, average maximum height attained);

b) mean observed minus first-guess geopotential height difference;

c) root mean square observed minus first-guess geopotential height difference;

d) root mean square observed minus first-guess vector wind difference.

In addition, several stations are examined more closely using tools such as long-term trend graphs and vertical profiles of observed minus first-guess differences.

4.1 Data availability

Figs. 4 and 5 display the reception rates at ECMWF from the North American radiosonde network at 100 hPa for 00 UTC and 12 UTC during the month of December 1986. The numbers plotted are the percentages of the total possible for that month and synoptic hour. Values are plotted for each station which should report at that hour, as specified in WMO Publication No. 9 Vol. A.

The 100 hPa height was received on more than 75% of occasions from most of the stations in the United States. The reception rate for many stations was slightly greater at 12 UTC than 00 UTC. However, several stations that should have reported at 12 UTC but not 00 UTC were not received at all.

Figs. 6 and 7 display the average maximum height (in kilometres) reached by the North American radiosonde network for 00 UTC and 12 UTC during the month of December 1986. Values are plotted for all stations received at least once during the month and refer to parts A and C of the TEMP reports only.

According to WMO regulations the height to be reached on a regular basis is 10 hPa (approximately 31 km) over the North American continent. The figures indicate that the majority of stations had an average value of around 23 km (approximately 30 hPa). There are a few stations with average heights well below the average, such as Bermuda (32°N 65°W) where, on average, 15-16 km (approximately 100 hPa) was reached.

4.2 Bias of height observations

As discussed in section 3, in data-rich areas such as the North American continent, the first-guess error of the ECMWF model is low, thereby allowing the evaluation of data quality by comparison with the 6-hour forecast. Figs. 8 and 9 display the observed minus first-guess differences at 100 hPa for 00 UTC and 12 UTC averaged over the month of December 1986. Assuming a low forecast error, these values represent the bias of the radiosonde observations at 100 hPa. Values are plotted for all stations received at least five times during the month and the units are metres.

Over USA at 00 UTC there is a clear division between positive biases in the west and negative biases in the east, closely corresponding to the division between daytime and night-time in December. At 12 UTC, when continental USA is almost completely in darkness in December, the bias values are uniformly negative. These figures confirm the findings by Nash (1984) and Lange (1987) that the North American radiosondes appear to have a uniform radiation error which should be corrected.

In order to study this effect more closely, we may investigate one particular station in more detail. Figs. 10 and 11 show the evolution of the mean monthly differences between observations and first-guess over the 13 month period December 1985 to December 1986 for the radiosonde station 72694 (Salem/McNary). Separate curves for 500 hPa, 100 hPa and 50 hPa are shown; 00 UTC and 12 UTC data are displayed in different figures. The number of observations shown above the time graph box are the number of 500 hPa height reports received during each month. The graphs clearly demonstrate the radiation correction problem, the bias being generally positive at 00 UTC and negative at 12 UTC throughout the year. It can also be seen that the magnitude of the bias increases with height. The period from December 1985 to April 1986 appears to have a different character from the rest of the year, particularly at 00 UTC. It is quite likely that this effect is due to a change made to the ECMWF operational forecast model in early May when three vertical levels were added in the stratosphere, thereby improving the resolution around the 50 hPa level.

4.3 Root mean square error of height observations

Figs. 12 and 13 display the root mean square (RMS) differences between observed values and the first-guess field of geopotential height at 100 hPa for 00 UTC and 12 UTC averaged over the month of December 1986. Values are plotted for all stations received at least 5 times during the month and the units are metres. The difference between the RMS values and the bias values gives an indication of the randomness of the observation error, i.e. if the RMS and bias values are very similar then most of the observation error is attributable to the bias.

It can be seen from Figs. 12 and 13 that most of the US stations had 100 hPa RMS errors in the order of 30-40 metres, and (referring to Figs. 8 and 9) most of this error was due to the large bias values. Some radiosonde stations, however, had RMS errors considerably larger than average, such as 72572 (Salt Lake City, 41°N 111°W) with a 100 hPa RMS error of 58 metres at 00 UTC. This station has been studied in more detail by looking at the evolution of the monthly RMS differences between observations and first-guess over the period December 1985 to December 1986 (Figs. 14 and 15). The explanation of the curves and number of observations displayed is the same as that for the time graphs of bias (see section 4.2). The 00 UTC graph clearly shows that in December 1986 there was a sharp rise in the RMS error at both 100 hPa and 50 hPa, whereas at 12 UTC there was no corresponding increase. The reason for this disparity can be discovered when the daily departures are examined. Fig. 16 depicts the time series of observed minus first-guess geopotential differences every 12 hours during December 1986 at 15 standard pressure levels from 1000 hPa to 10 hPa. The differences are in metres with a scale of 50 m indicated by dots for each level. The mean deviation over the month is printed on the right hand side of each time series, together with the two values of mean ± 50 m. A star at the observation time indicates that the observation was presented to the analysis. If a datum was rejected by the quality control procedure within the analysis program a "flag" of 2 (= probably incorrect) or 3 (= incorrect) is also indicated by "A = 2" or "A = 3" printed at the time and level affected. It can be seen from the figure that at 00 UTC December 21 there was an exceptionally large deviation from the first-guess, which almost certainly caused the sharp rise in RMS error observed in Fig. 14. Another interesting feature shown in the graph for 00 UTC is the annual cycle in the 500 hPa RMS, reaching a peak in the summer months. This is almost certainly linked to the bias correction problem discussed in section 4.2, although it is not clear why a similar effect is not evident at 12 UTC.

4.4 Individual station investigation

In this section selected radiosonde stations are investigated more closely using two more tools:

a) long-term trend graphs of vertically averaged statistics, and

b) vertical profiles of observed minus first-guess and analysis differences.

For vertically averaged statistics, the differences at each of the 10 standard levels between 1000 hPa and 100 hPa are weighted by the normalised inverse of the RMS observation errors for radiosonde observations as used in the Centre's data assimilation scheme and given below:

Inst.Type	1000	850	750	500	400	300	250	200	150	100
SONDE/WIND (m/s)	2.2	2.5	2.6	3.1	3.7	3.8	3.3	3.0	2.8	2.4
SONDE/GEOP. (m)	5.0	5.4	6.0	9.4	11.6	13.8	14.2	15.2	18.2	21.4

Graphs labelled RMS give the RMS differences between observations and first-guess. The BIAS curves show the evolution of the mean monthly differences between observations and the first guess over the 13 month period. Results are shown for 00 and 12 UTC separately. The number of observations (part A of the TEMP) received during each month is indicated above the time graph box.

In the vertical profiles the differences between height and wind observations and the ECMWF first guess and analysis (interpolated to the location of the station) are presented for each of the standard pressure levels. The figures give standard deviation (left) and bias (right) of u-component (top), v-component (centre) and geopotential height (bottom) of the differences in the units ms^{-1} for wind and m for height. The numbers in the centre give the number of observations used for the calculations (TEMP/PILOT). Dashed lines denote deviations from the uninitialised analysis, solid lines deviations from the first-guess fields.

In Figs. 17 and 18 an example of a well-performing station is shown - 72528 (Buffalo). Looking first at the long-term trend graph it is clear that both the mean error (bias) and RMS error were uniformly low throughout 1986. There is slight evidence for an annual cycle in the bias, being generally positive during the summer months and negative for the remainder of the year, although the absolute values were very small. Fig. 18 shows the vertical profile of observed minus first-guess and analysis differences for June 1986. The geopotential height profiles (bottom) indicate that the bias was very low throughout the depth of the atmosphere, although at 12 UTC a slight positive bias is evident in the upper troposphere and a larger positive bias in the upper stratosphere.

A contrasting case is shown in Figs. 19 and 20, that of 78016 (Bermuda). The long-term trend graph (Fig. 19) shows that the vertically averaged RMS error never fell below 25 m and for most of the year was around 30 to 40 m. A marked peak in the RMS error occurred in August, corresponding with a negative peak in the bias. An annual cycle is evident in the bias with large positive values during the winter months. Looking at January 1986 in more detail the vertical profiles of geopotential (bottom of Fig. 20) show clearly the uniform positive bias in the troposphere.

An example of a station exhibiting a marked bias correction problem is given in Figs. 21 and 22. Station number 91285 (Hilo/Gen. Lyman, Hawaii) had a positive bias at 00 UTC and a negative bias at 12 UTC (apart from December 1986). It can be seen that the bias makes up the greater part of the observation error as the RMS error shows only a small increase over the bias. The character of the bias profile can be seen clearly in Fig. 22 which shows the results for July 1986.

4.5 Root mean square error of wind observations

Figs. 23 and 24 display the root mean square (RMS) vector differences between observed values and the first-guess field of 250 hPa wind for 00 UTC and 12 UTC averaged over the month of December 1986. Values are plotted for all stations received at least 5 times during the month and the units are metres per second.

It can be seen that most of the stations in the USA had RMS vector wind errors of the order 6 to 8 m s^{-1}, although a few performed significantly worse than average having errors greater than 10 m s^{-1}.

5. ACKNOWLEDGEMENT

The contributions by F. Delsol, A. Lange and H. Pümpel at an earlier stage of the project are gratefully acknowledged.

6. REFERENCES

ECMWF, 1987: Planning meeting on data for global models, Final Report

Hollingsworth, A., Shaw, D.B., Lönnberg, P., Illari, L., Arpe, K., and Simmons, A.J., 1986: Monitoring of Observation and Analysis Quality by a Data Assimilation System. Mon.Wea.Rev. 114, 861-879

Jarraud, M., Simmons, A.J., Kanamitsu, M., 1985: Development of the high resolution model. ECMWF Technical Memorandum No. 107 (available from ECMWF)

Lange, A.A., 1987: A High-Pass Filter for Optimum Calibration of Observing Systems with Applications to: The Multi-Path Propagation Problem with the VLF Navaids, Wind-Tracking with a Hybrid System, and The Systematic Errors of the Global Observing System (GOS). Submitted for publication in the proceedings of the IMA Conference on Simulation and Optimisation of Large Systems, University of Reading. 23-25 September, 1986, to be published by Oxford University Press in 1987.

Lönnberg, P., Pailleux, J., and Hollingsworth, A., 1986: The new analysis system. ECMWF Technical Memorandum No. 125 (available from ECMWF)

Lönnberg, P., and Shaw, D.B., 1985: Data selection and quality control in the ECMWF analysis system. Proc. ECMWF Workshop on the Quality and Use of Meteorological Observations, 225-254 (available from ECMWF)

Lorenc, A.C., 1981: A Global Three-dimensional Multivariate Statistical Interpretation Scheme. Mon.Wea.Rev., 109, 701-721

Nash, J., 1984: Compatability of radiosonde measurements in the upper troposphere and lower stratosphere for the period 1/11/1981 to 31/10/1982. O.S.M. 24 Meteorological Office, Bracknell, U.K.

Shaw, D.B., Lönnberg, P., Hollingsworth, A., 1984: The 1984 revision of the ECMWF analysis system. Technical Memorandum No. 92 (available from ECMWF)

Simmons, A.J., and Jarraud, M., 1983: The design and performance of the new ECMWF operational model. Proceedings of the 1983 ECMWF Seminar.

Tiedtke, M., Geleyn, J.-F., Hollingsworth, A., and Louis, J.-F., 1979: ECMWF model parameterisation of sub grid scale processes. ECMWF Tech. Rep. 10 (available from ECWMF)

Tiedtke, M., and Slingo, J., 1985: Development of the operational parameterization scheme. ECMWF Technical Memorandum No. 108 (available from ECMWF).

WMO, 1985: Commission for Basic Systems, Abridged Final Report of the Extraordinary Session, Hamburg 1985

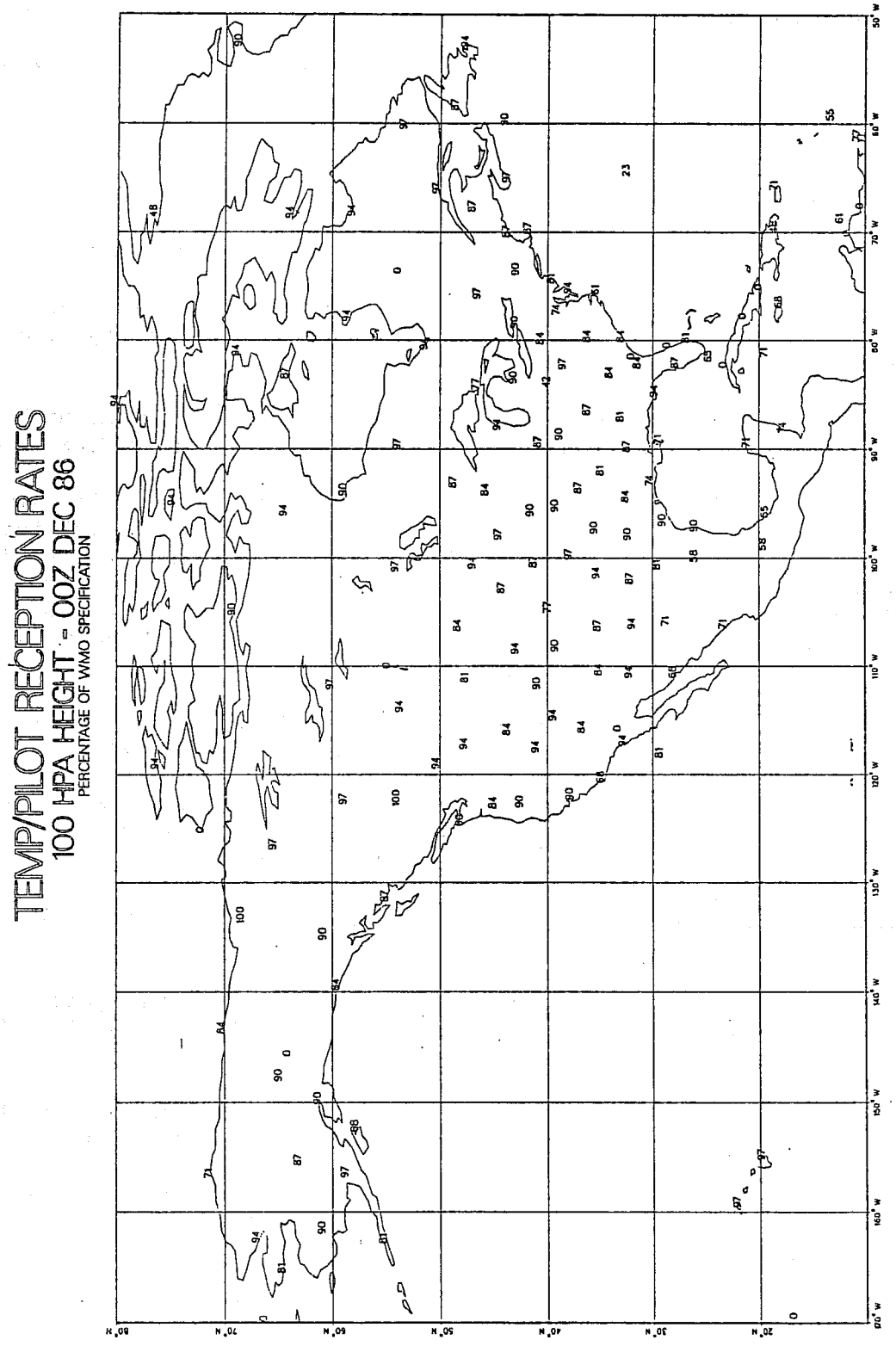
TEMP/PILOT RECEPTION RATES
100 HPA HEIGHT - 00Z DEC 86
PERCENTAGE OF WMO SPECIFICATION

Fig. 4

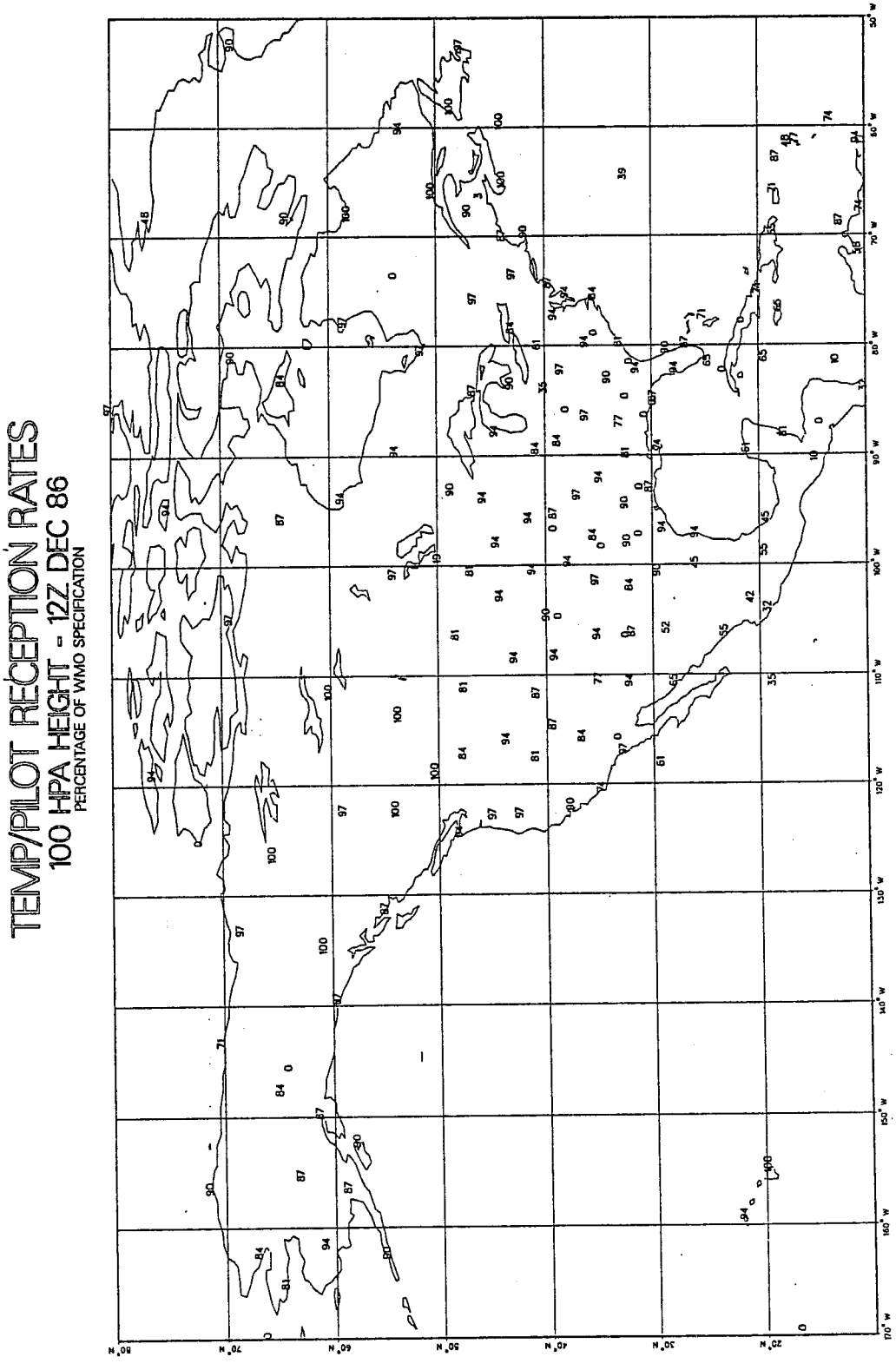
TEMP/PILOT RECEPTION RATES
100 HPA HEIGHT - 12Z DEC 86
PERCENTAGE OF WMO SPECIFICATION

Fig. 5

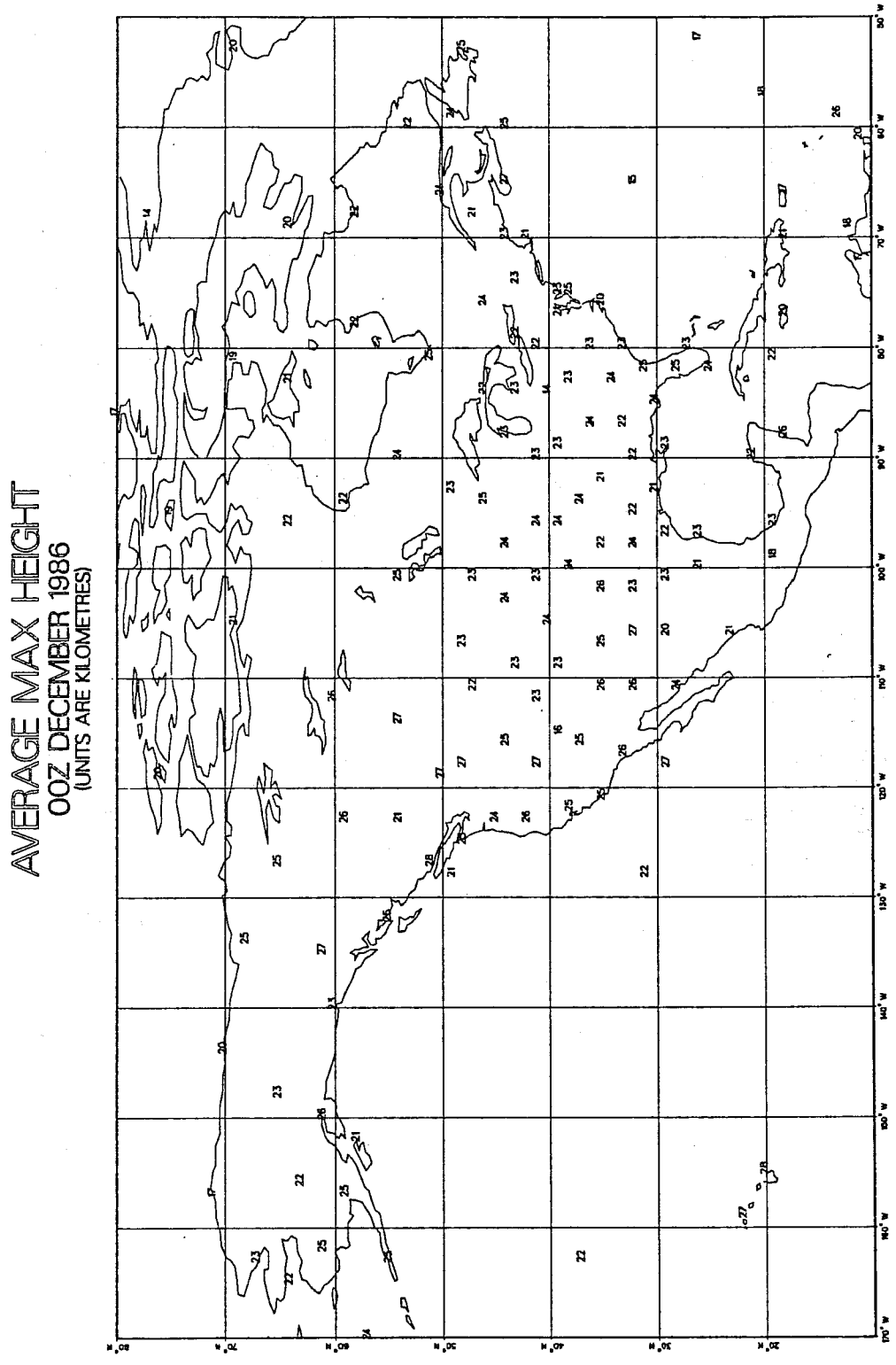

Fig. 6

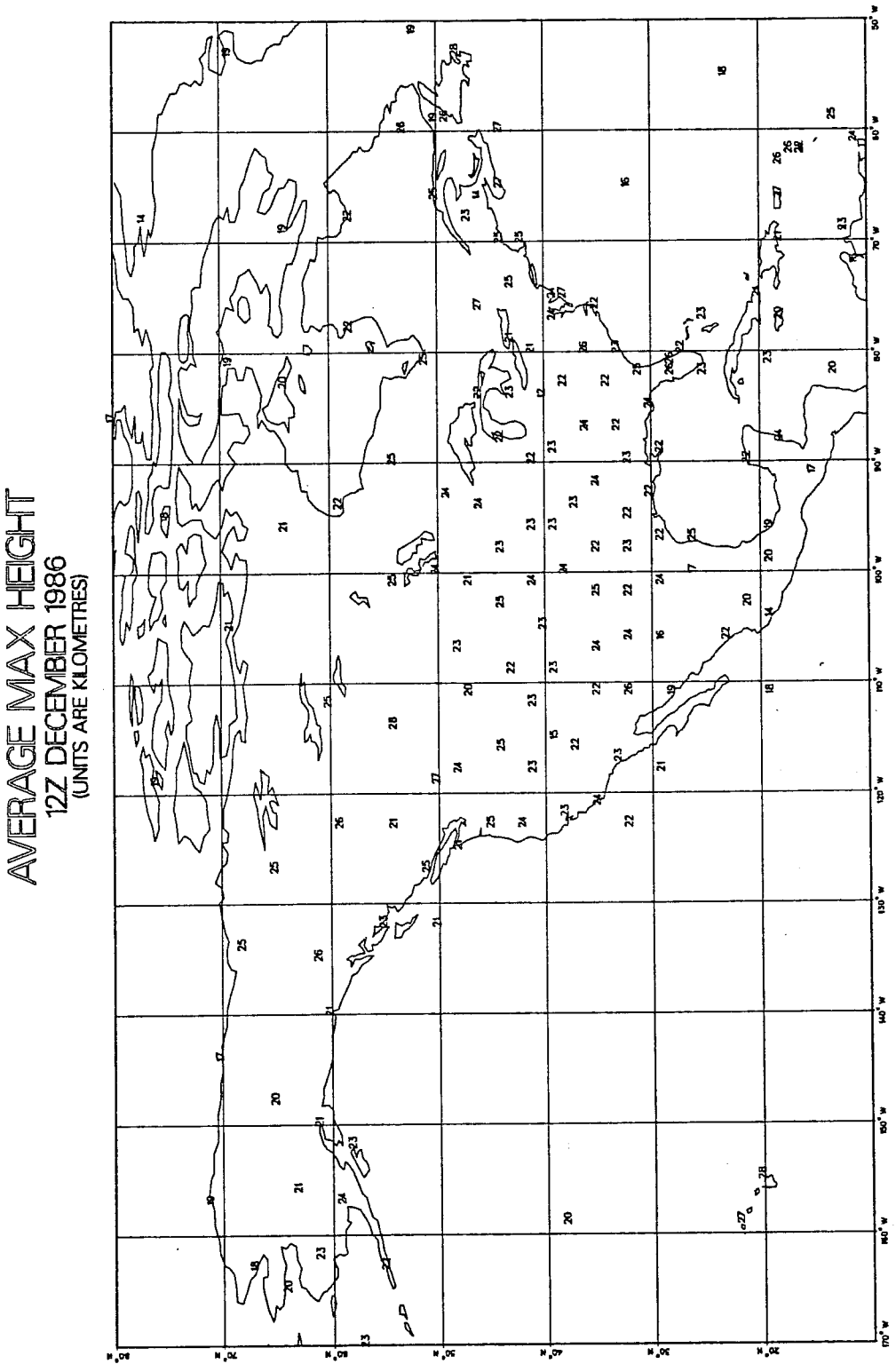

Fig. 7

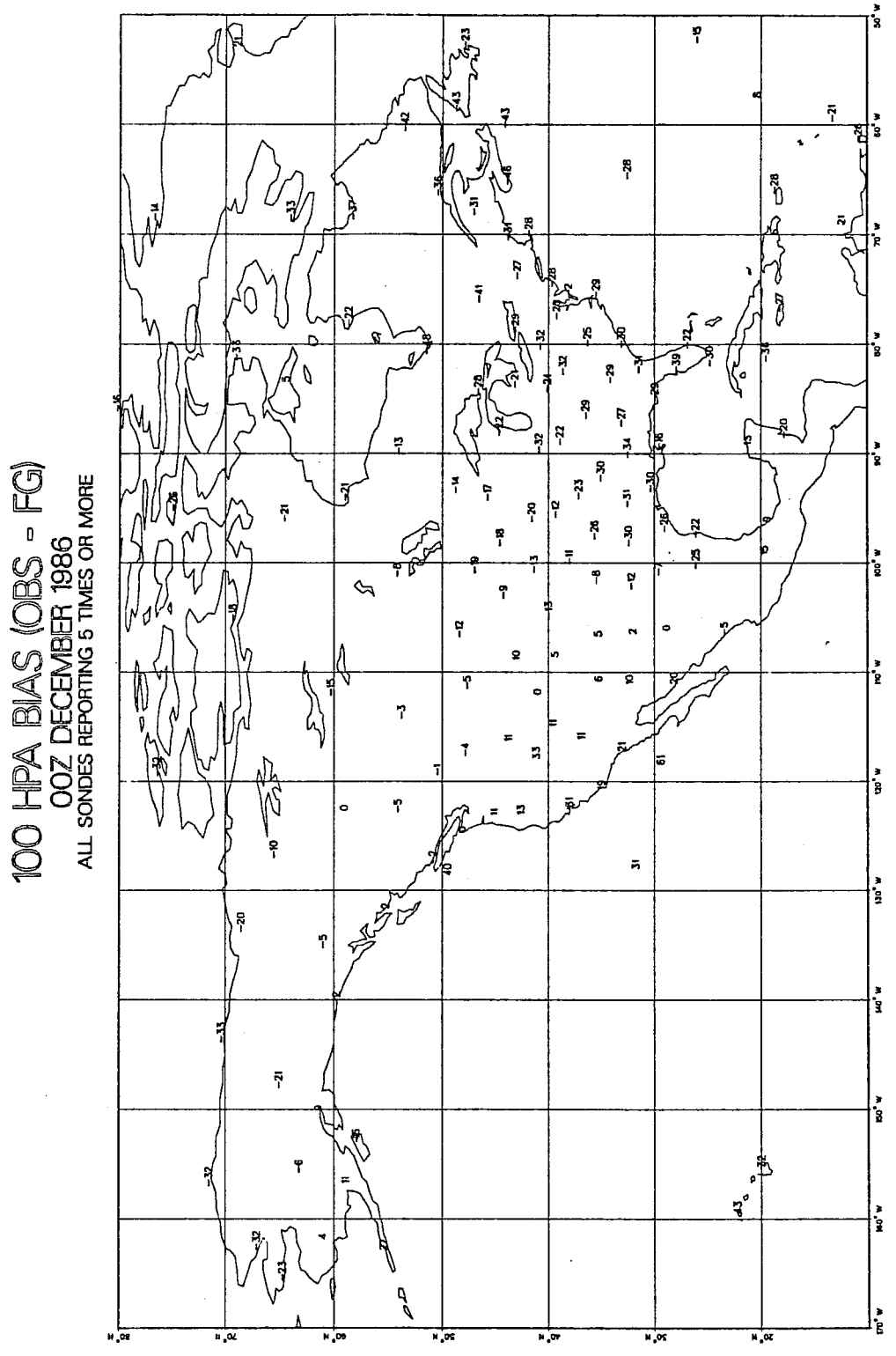
100 HPA BIAS (OBS - FG)
00Z DECEMBER 1986
ALL SONDES REPORTING 5 TIMES OR MORE

Fig. 8

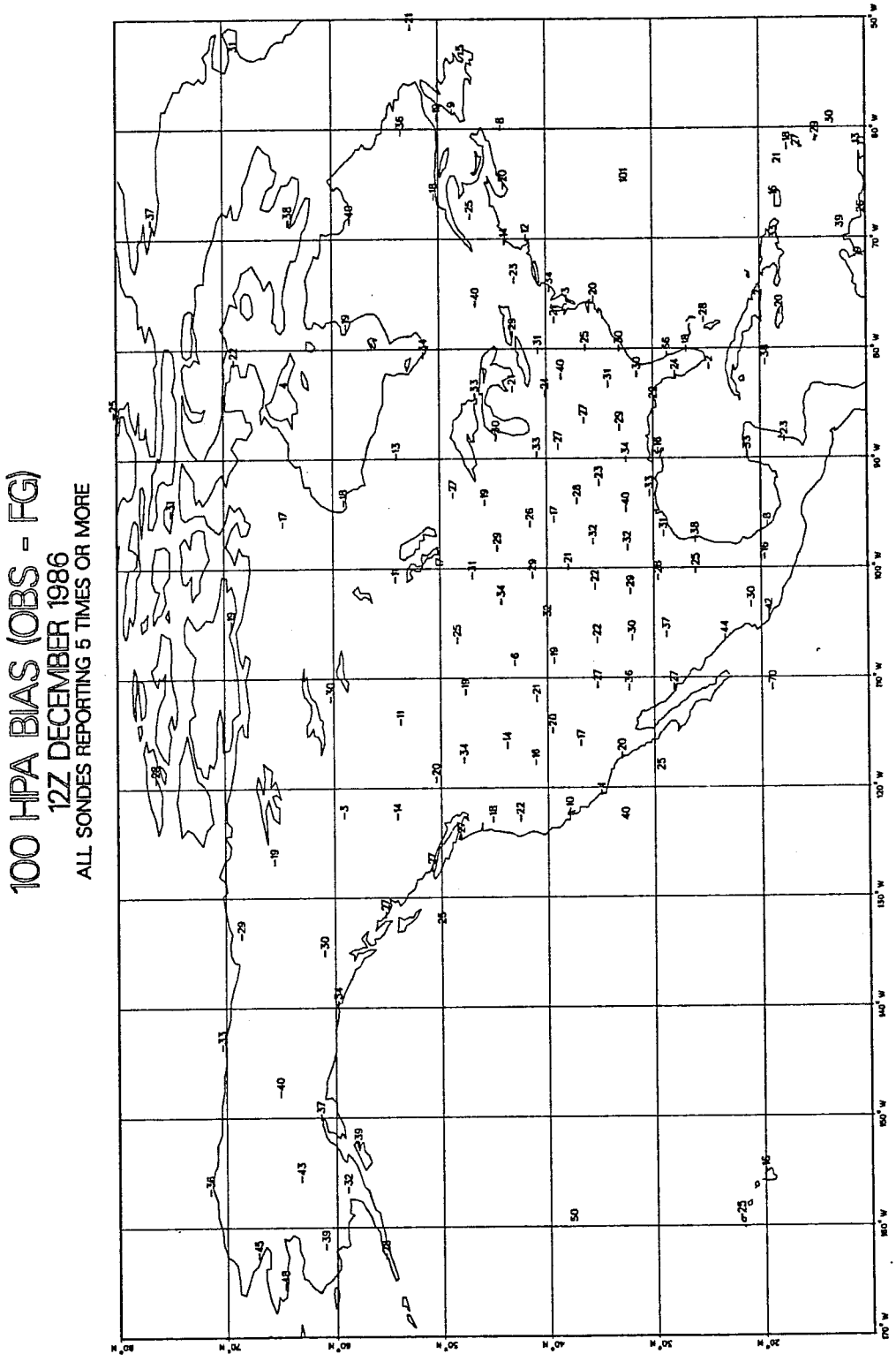
100 HPA BIAS (OBS - FG)
12Z DECEMBER 1986
ALL SONDES REPORTING 5 TIMES OR MORE

Fig. 9

Fig. 10

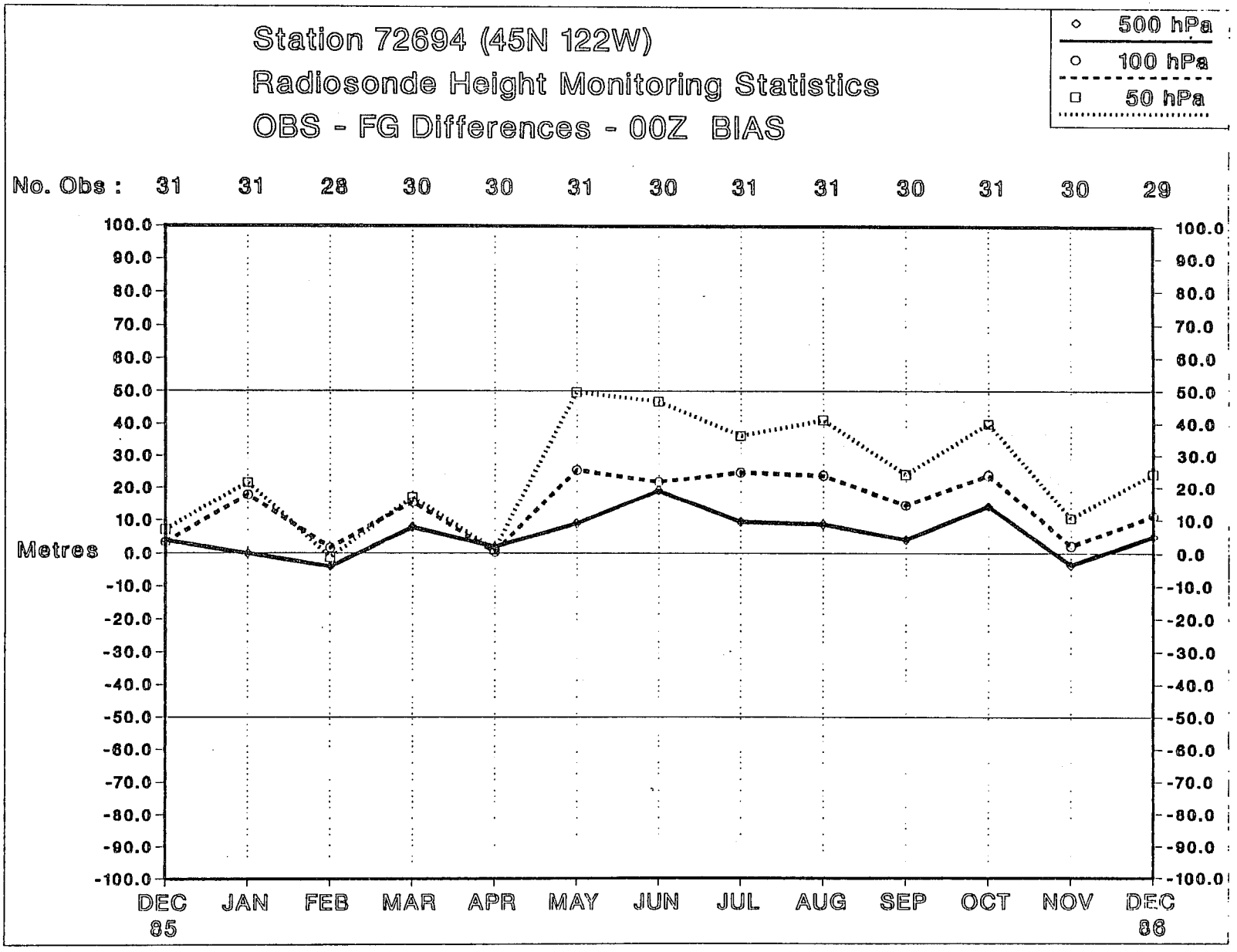
Station 72694 (45N 122W)
Radiosonde Height Monitoring Statistics
OBS - FG Differences - 00Z BIAS
500 hPa
100 hPa
50 hPa
No. Obs : 31 31 28 30 30 31 30 31 31 30 31 30 29
Metres
100.0
90.0
80.0
70.0
60.0
50.0
40.0
30.0
20.0
10.0
0.0
-10.0
-20.0
-30.0
-40.0
-50.0
-60.0
-70.0
-80.0
-90.0
-100.0
DEC 85
JAN
FEB
MAR
APR
MAY
JUN
JUL
AUG
SEP
OCT
NOV
DEC 86

Fig. 11

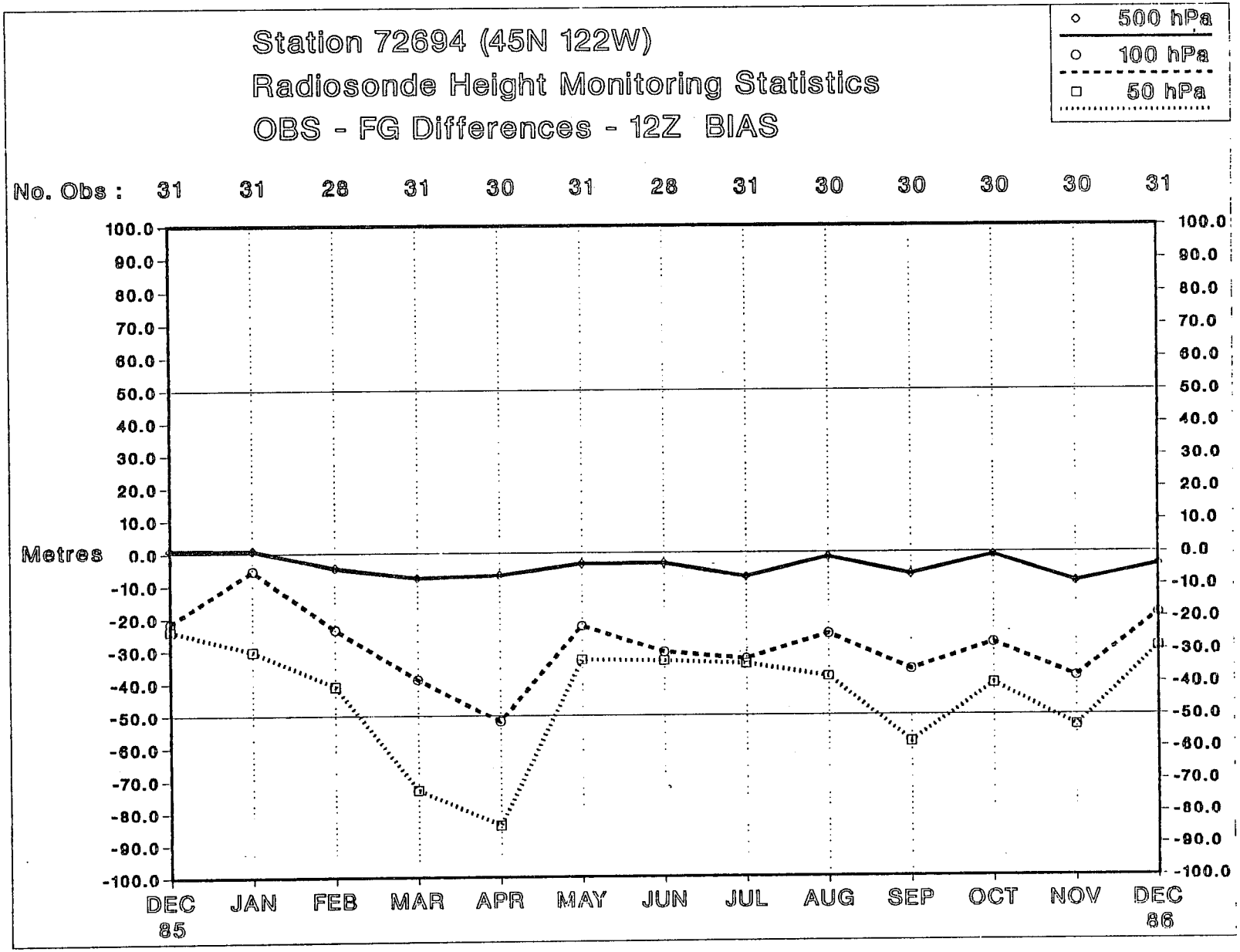
Station 72694 (45N 122W)
Radiosonde Height Monitoring Statistics
OBS - FG Differences - 12Z BIAS
500 hPa
100 hPa
50 hPa
No. Obs : 31 31 28 31 30 31 28 31 30 30 30 30 31
Metres
100.0
90.0
80.0
70.0
60.0
50.0
40.0
30.0
20.0
10.0
0.0
-10.0
-20.0
-30.0
-40.0
-50.0
-60.0
-70.0
-80.0
-90.0
-100.0
DEC 85
JAN
FEB
MAR
APR
MAY
JUN
JUL
AUG
SEP
OCT
NOV
DEC 86

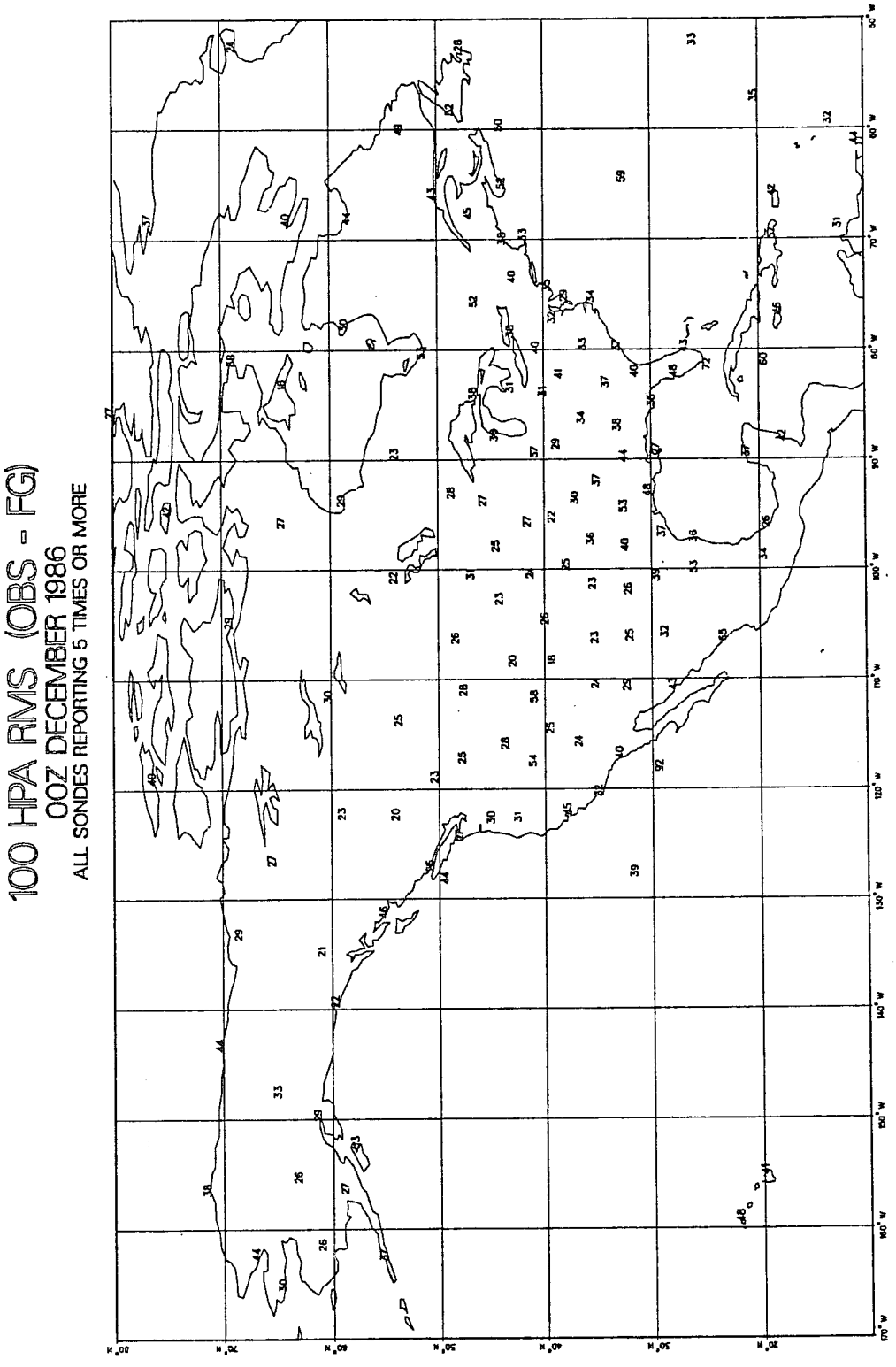
100 HPA RMS (OBS - FG)
00Z DECEMBER 1986
ALL SONDES REPORTING 5 TIMES OR MORE

Fig. 12

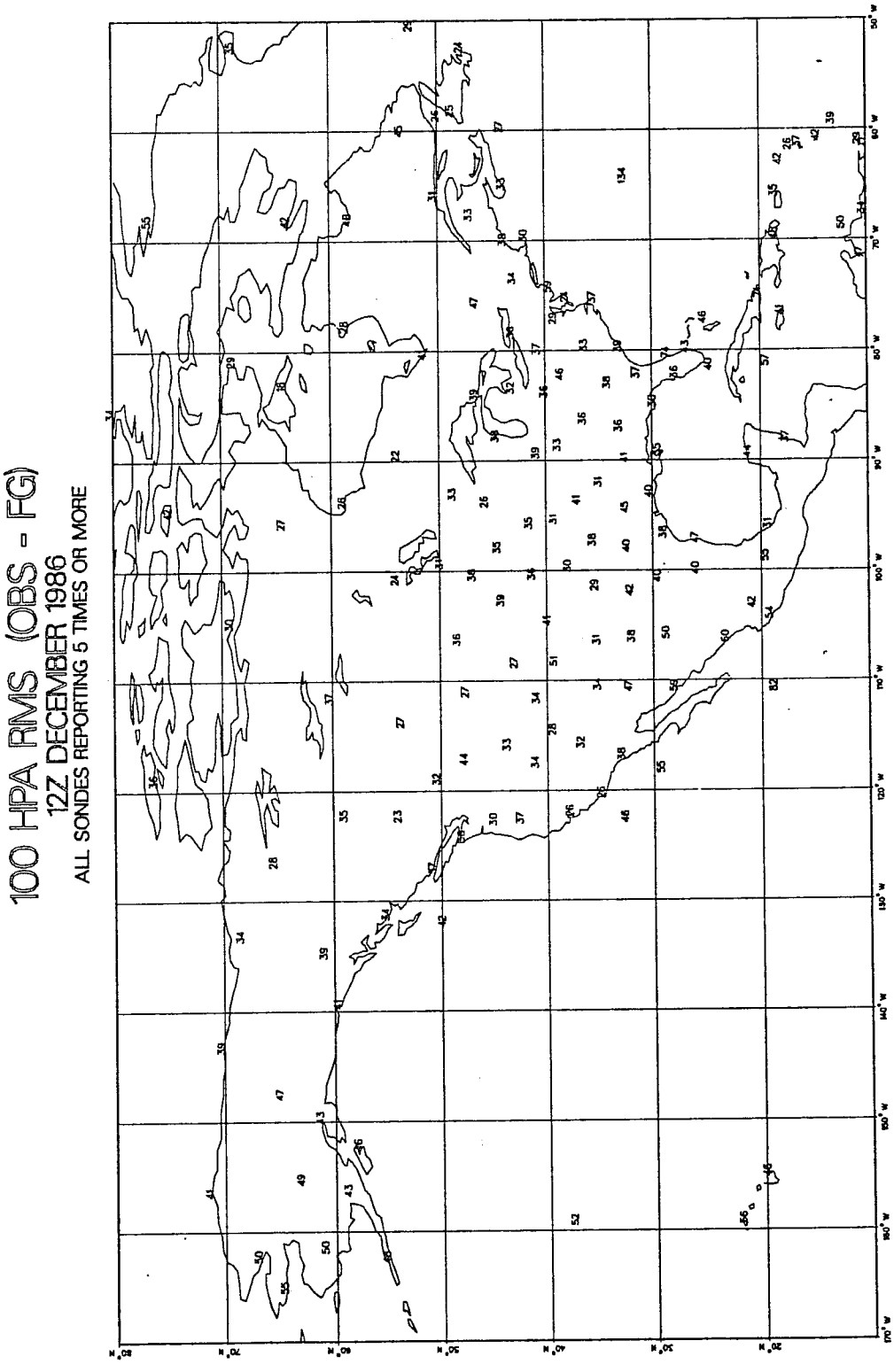
100 HPA RMS (OBS - FG)
12Z DECEMBER 1986
ALL SONDES REPORTING 5 TIMES OR MORE

Fig. 13

Fig. 14

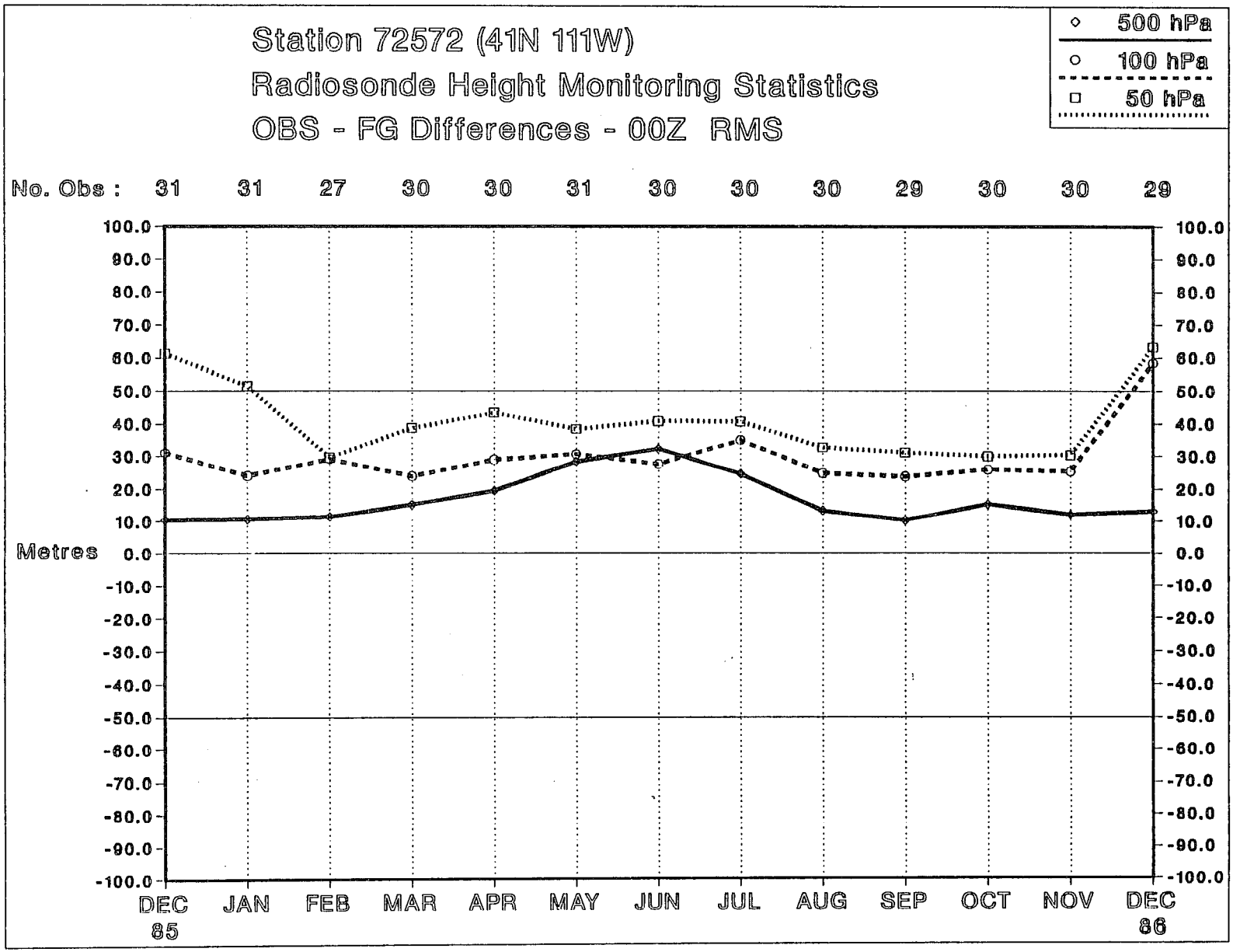
Station 72572 (41N 111W)
Radiosonde Height Monitoring Statistics
OBS - FG Differences - 00Z RMS
500 hPa
100 hPa
50 hPa
No. Obs : 31 31 27 30 30 31 30 30 30 29 30 30 29
Metres
100.0
90.0
80.0
70.0
60.0
50.0
40.0
30.0
20.0
10.0
0.0
-10.0
-20.0
-30.0
-40.0
-50.0
-60.0
-70.0
-80.0
-90.0
-100.0
DEC 85
JAN
FEB
MAR
APR
MAY
JUN
JUL
AUG
SEP
OCT
NOV
DEC 86

Fig. 15

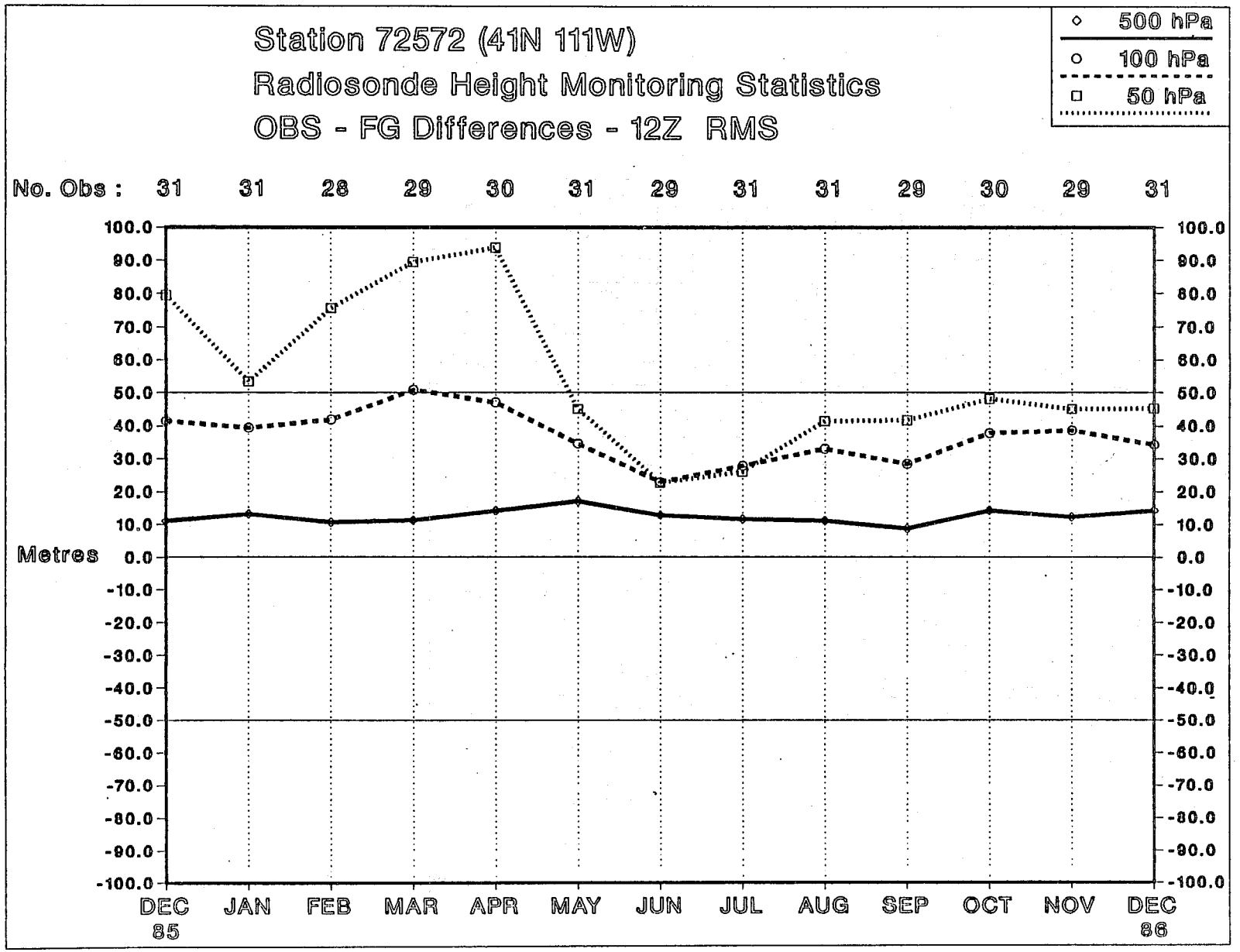
Station 72572 (41N 111W)
Radiosonde Height Monitoring Statistics
OBS - FG Differences - 12Z RMS
500 hPa
100 hPa
50 hPa
No. Obs : 31 31 28 29 30 31 29 31 31 29 30 29 31
Metres
100.0
90.0
80.0
70.0
60.0
50.0
40.0
30.0
20.0
10.0
0.0
-10.0
-20.0
-30.0
-40.0
-50.0
-60.0
-70.0
-80.0
-90.0
-100.0
DEC 85
JAN
FEB
MAR
APR
MAY
JUN
JUL
AUG
SEP
OCT
NOV
DEC 86

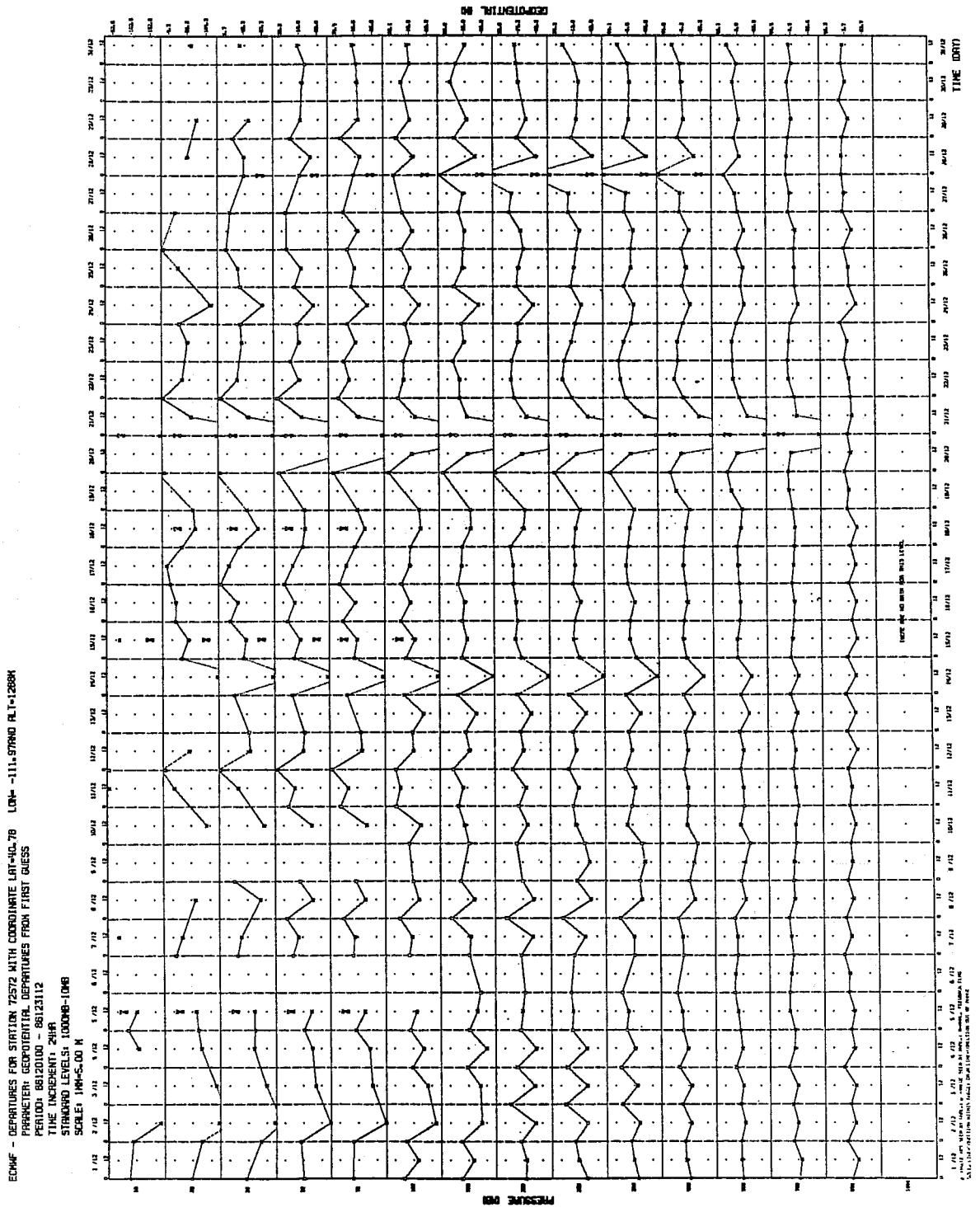

Fig. 16 Daily departures from first guess, December 1986, station 72572

Fig. 17

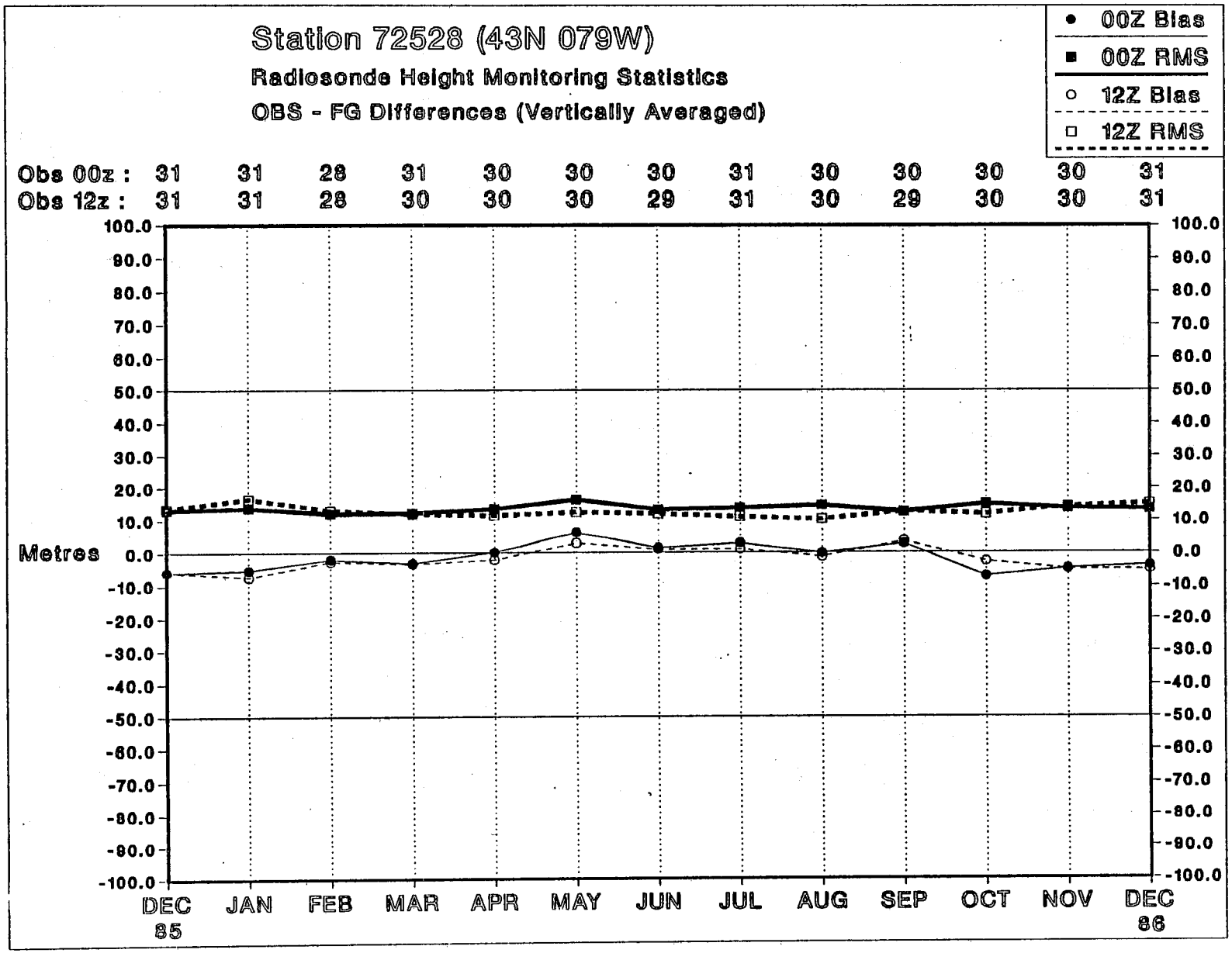
Station 72528 (43N 079W)
Radiosonde Height Monitoring Statistics
OBS - FG Differences (Vertically Averaged)
00Z Bias
00Z RMS
12Z Bias
12Z RMS
Obs 00z : 31 31 28 31 30 30 30 31 30 30 30 30 31
Obs 12z : 31 31 28 30 30 30 29 31 30 29 30 30 31
Metres
100.0
90.0
80.0
70.0
60.0
50.0
40.0
30.0
20.0
10.0
0.0
-10.0
-20.0
-30.0
-40.0
-50.0
-60.0
-70.0
-80.0
-90.0
-100.0
DEC 85
JAN
FEB
MAR
APR
MAY
JUN
JUL
AUG
SEP
OCT
NOV
DEC 86

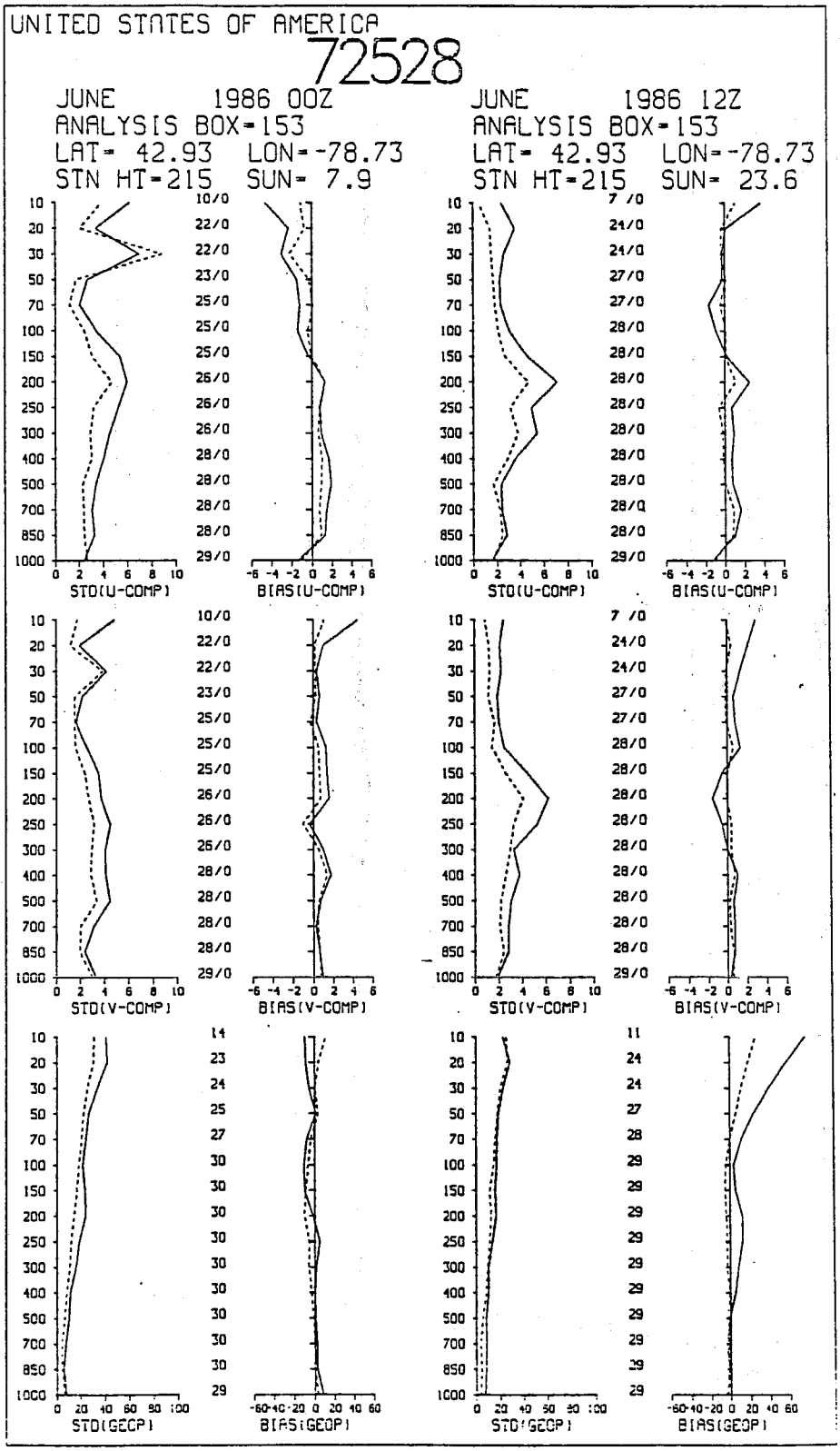
UNITED STATES OF AMERICA
72528
JUNE 1986 00Z
ANALYSIS BOX=153
LAT= 42.93 LON=-78.73
STN HT=215 SUN= 7.9
JUNE 1986 12Z
ANALYSIS BOX=153
LAT= 42.93 LON=-78.73
STN HT=215 SUN= 23.6
STD(U-COMP)
BIAS(U-COMP)
STD(V-COMP)
BIAS(V-COMP)
STD(GEOP)
BIAS(GEOP)

Fig. 18

Fig. 19

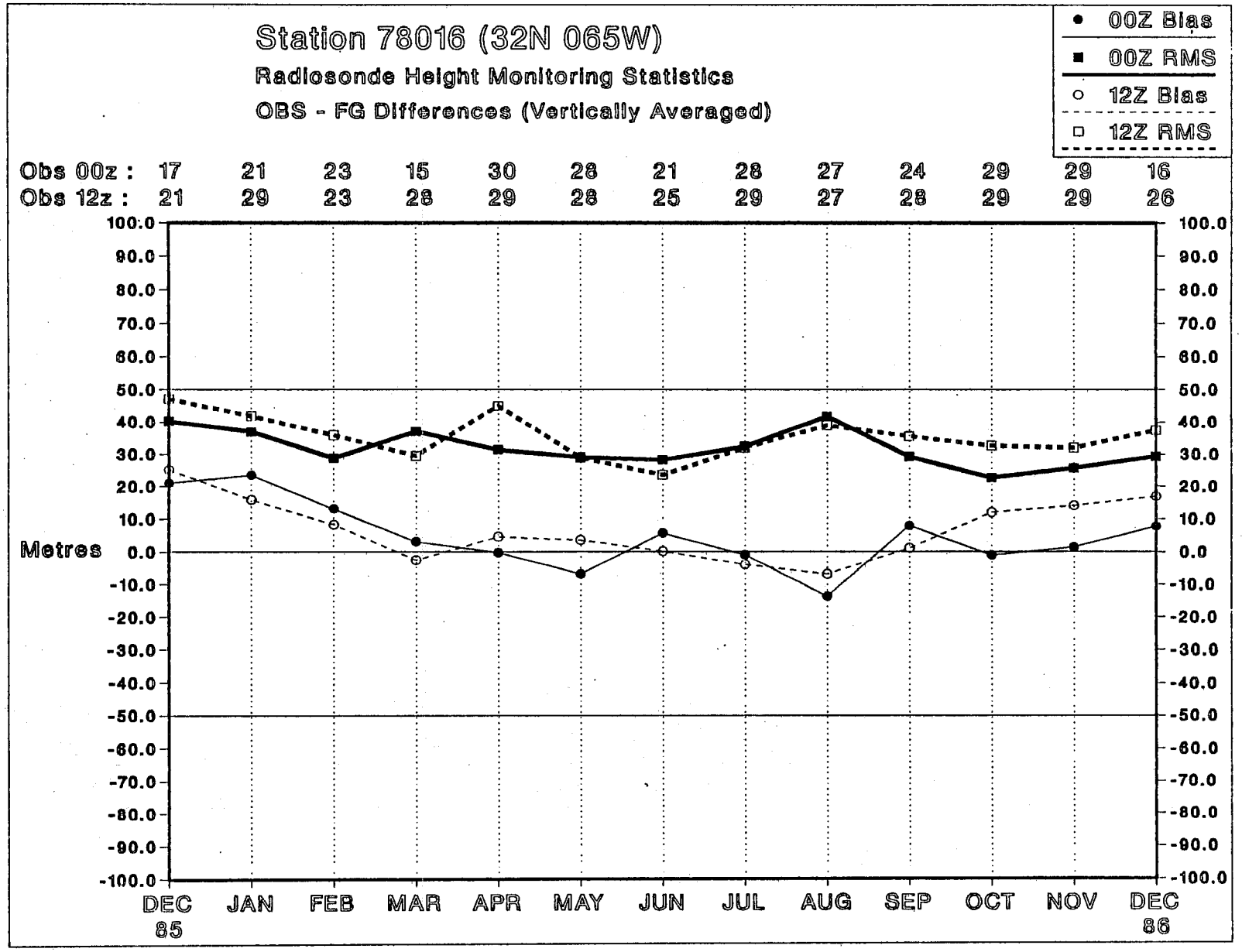
Station 78016 (32N 065W)
Radiosonde Height Monitoring Statistics
OBS - FG Differences (Vertically Averaged)
00Z Bias
00Z RMS
12Z Bias
12Z RMS
Obs 00z : 17 21 23 15 30 28 21 28 27 24 29 29 16
Obs 12z : 21 29 23 28 29 28 25 29 27 28 29 29 26
Metres
100.0
90.0
80.0
70.0
60.0
50.0
40.0
30.0
20.0
10.0
0.0
-10.0
-20.0
-30.0
-40.0
-50.0
-60.0
-70.0
-80.0
-90.0
-100.0
DEC 85
JAN
FEB
MAR
APR
MAY
JUN
JUL
AUG
SEP
OCT
NOV
DEC 86

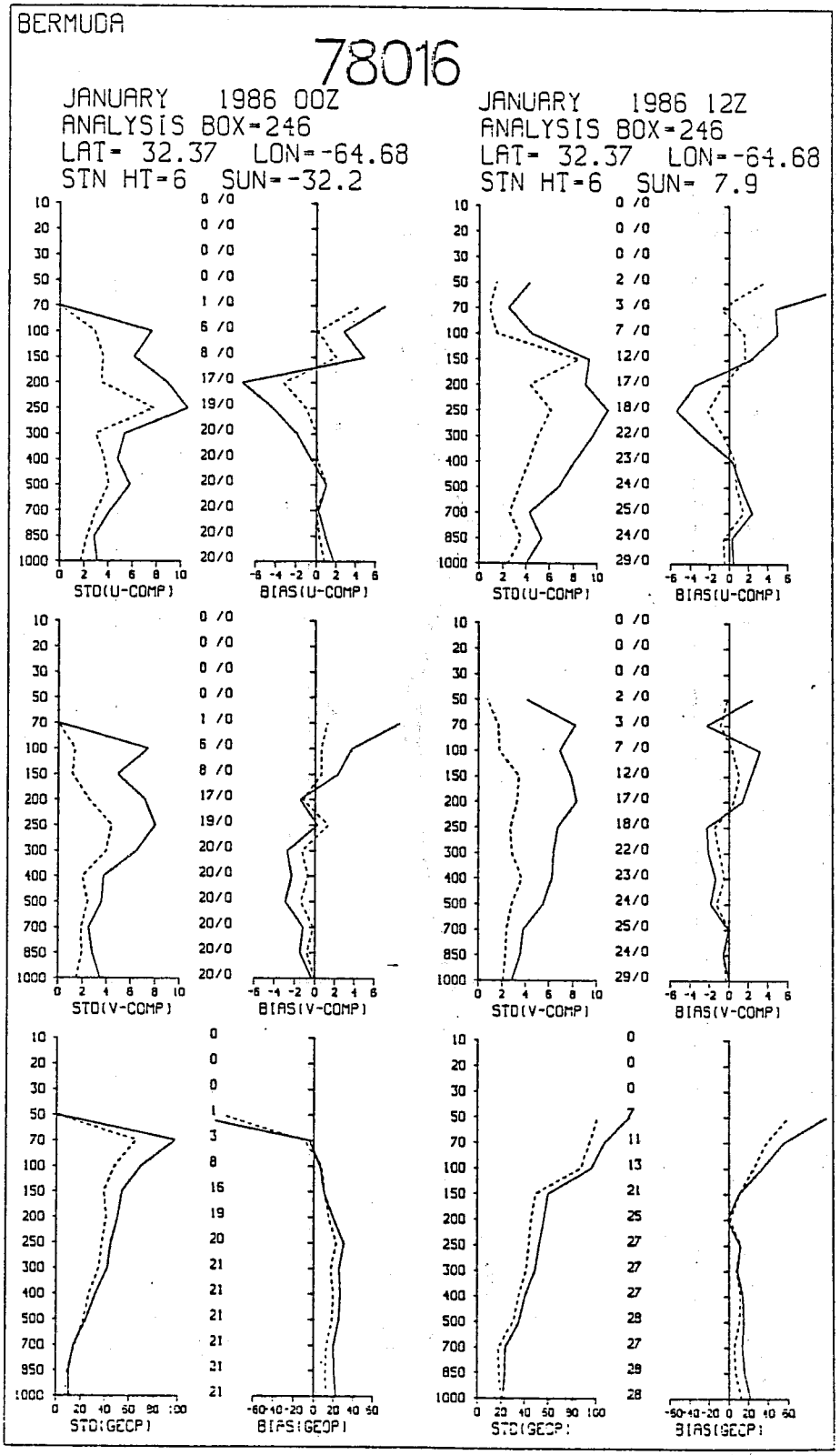
BERMUDA
78016
JANUARY 1986 00Z
ANALYSIS BOX=246
LAT= 32.37 LON=-64.68
STN HT=6 SUN=-32.2
JANUARY 1986 12Z
ANALYSIS BOX=246
LAT= 32.37 LON=-64.68
STN HT=6 SUN= 7.9
STD(U-COMP)
BIAS(U-COMP)
STD(V-COMP)
BIAS(V-COMP)
STD(GEOP)
BIAS(GEOP)

Fig. 20

Fig. 21

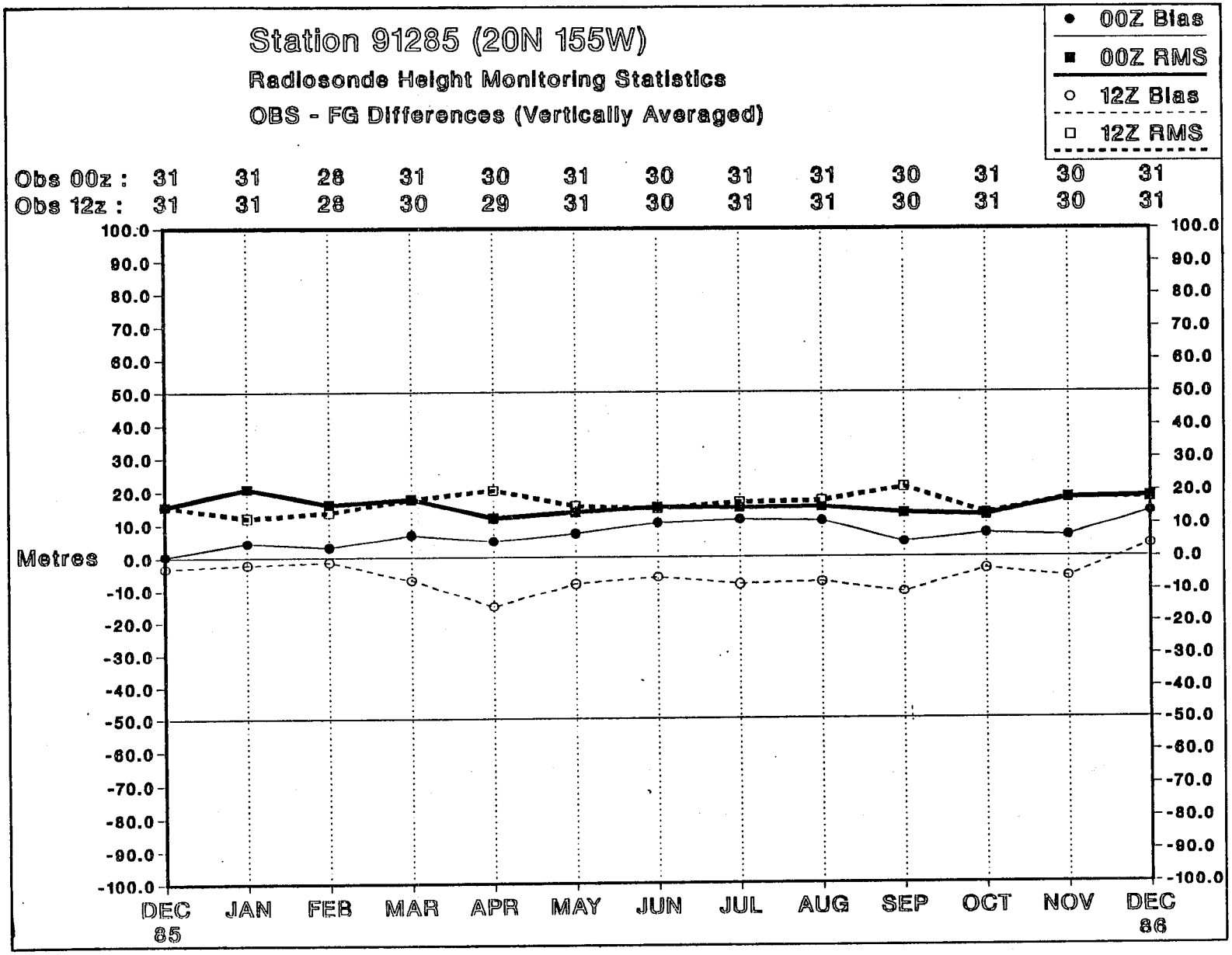
Station 91285 (20N 155W)
Radiosonde Height Monitoring Statistics
OBS - FG Differences (Vertically Averaged)
00Z Bias
00Z RMS
12Z Bias
12Z RMS
Obs 00z : 31 31 28 31 30 31 30 31 31 30 31 30 31
Obs 12z : 31 31 28 30 29 31 30 31 31 30 31 30 31
Metres
100.0
90.0
80.0
70.0
60.0
50.0
40.0
30.0
20.0
10.0
0.0
-10.0
-20.0
-30.0
-40.0
-50.0
-60.0
-70.0
-80.0
-90.0
-100.0
DEC 85
JAN
FEB
MAR
APR
MAY
JUN
JUL
AUG
SEP
OCT
NOV
DEC 86

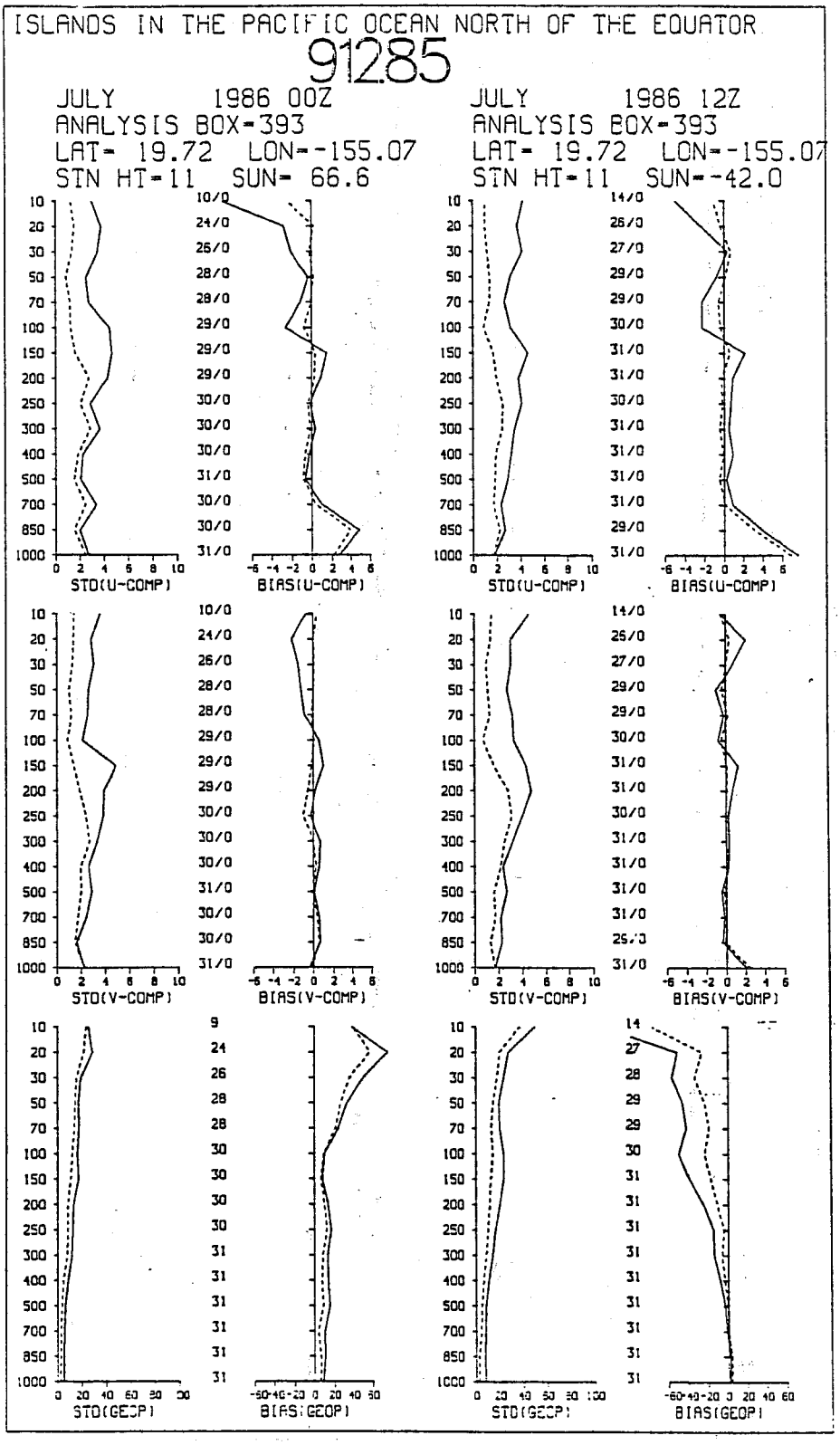
ISLANDS IN THE PACIFIC OCEAN NORTH OF THE EQUATOR
91285
JULY 1986 00Z
ANALYSIS BOX=393
LAT= 19.72 LON=-155.07
STN HT=11 SUN= 66.6
JULY 1986 12Z
ANALYSIS BOX=393
LAT= 19.72 LON=-155.07
STN HT=11 SUN=-42.0
STD(U-COMP)
BIAS(U-COMP)
STD(V-COMP)
BIAS(V-COMP)
STD(GEOP)
BIAS(GEOP)

Fig. 22

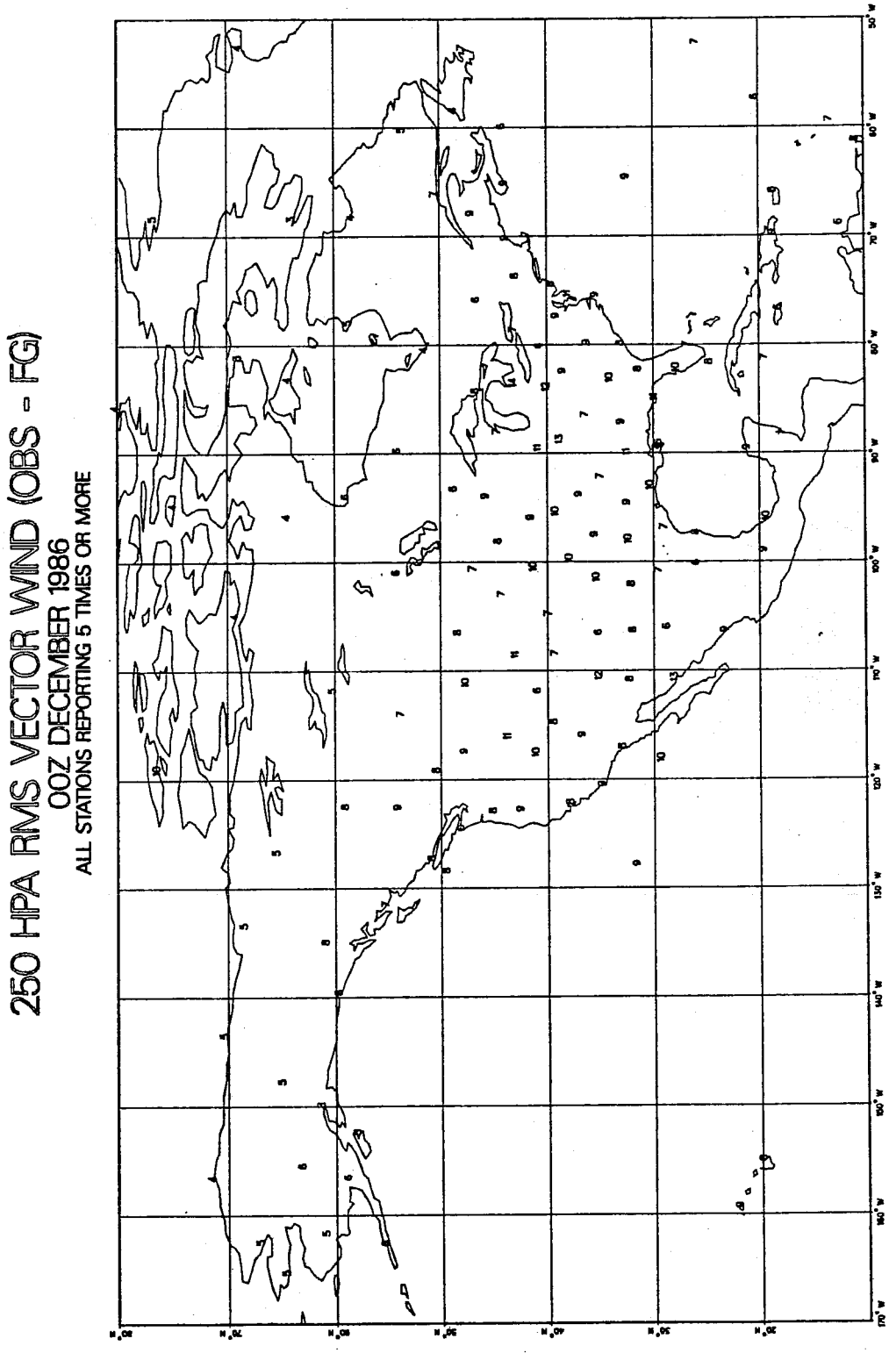
250 HPA RMS VECTOR WIND (OBS - FG)
00Z DECEMBER 1986
ALL STATIONS REPORTING 5 TIMES OR MORE

Fig. 23

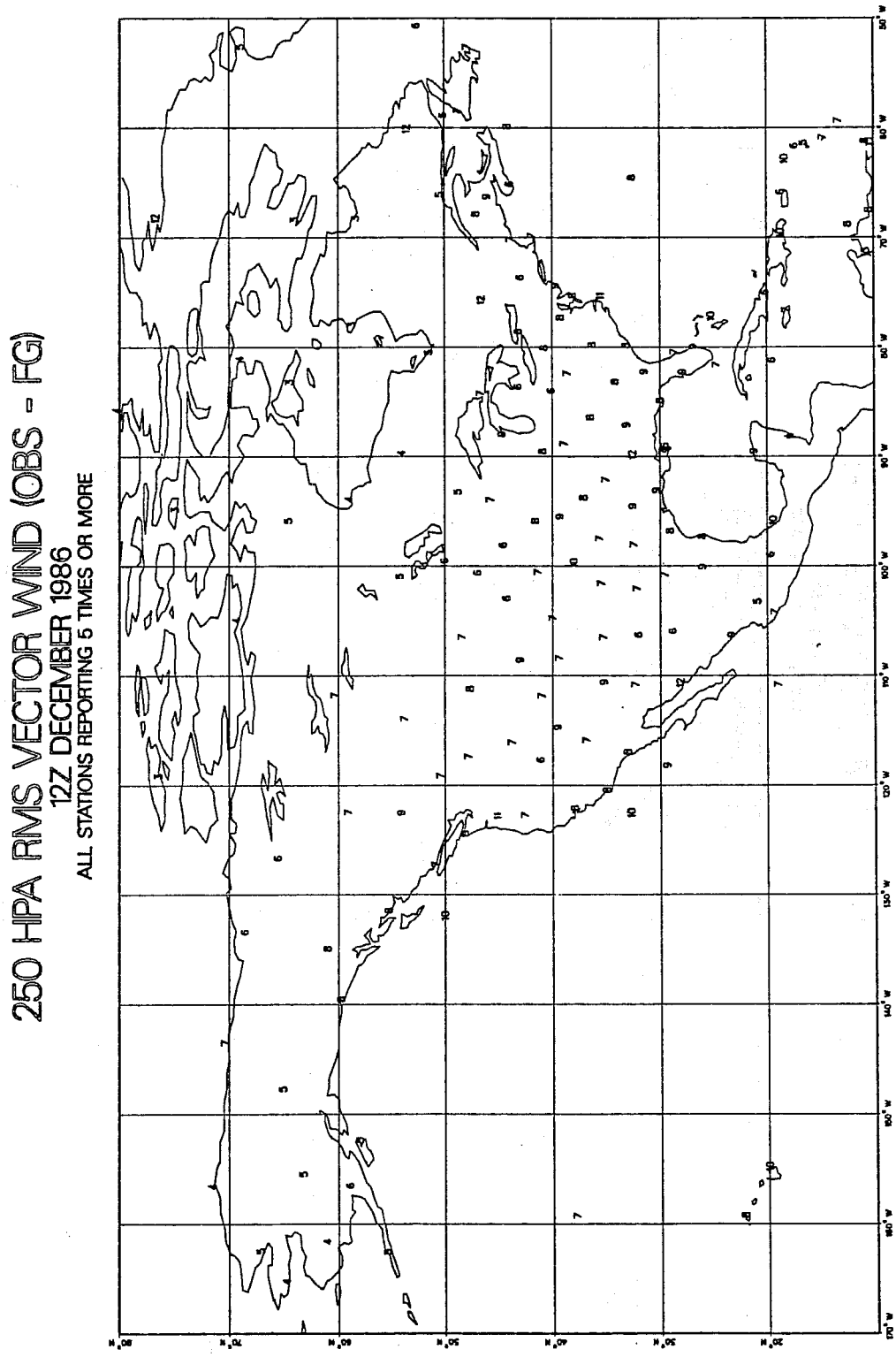
250 HPA RMS VECTOR WIND (OBS - FG)
12Z DECEMBER 1986
ALL STATIONS REPORTING 5 TIMES OR MORE

Fig. 24